

Supplementary Information

Trimerized Small-Molecule Acceptors Enable High-Performance Organic Solar Cells with High Open-Circuit Voltage and Prolonged Life-Time

Jin-Woo Lee^{†,a}, Cheng Sun^{†,b,c}, Tan Ngoc-Lan Phan^a, Dong Chan Lee^d, Zhengping Tan^a, Hyesu

Jeon^a, Shinuk Cho^d, Soon-Ki Kwon^e, Yun-Hi Kim^{c,*}, and Bumjoon J. Kim^{a,*}

^a Department of Chemical and Biomolecular Engineering, Korea Advanced Institute of Science and Technology (KAIST), Daejeon 34141, Republic of Korea

^b Qingdao Institute of Bioenergy and Bioprocess Technology, Chinese Academy of Sciences, Qingdao, 266101 China

^c Department of Chemistry and RINS, Gyeongsang National University, Jinju 52828, Republic of Korea

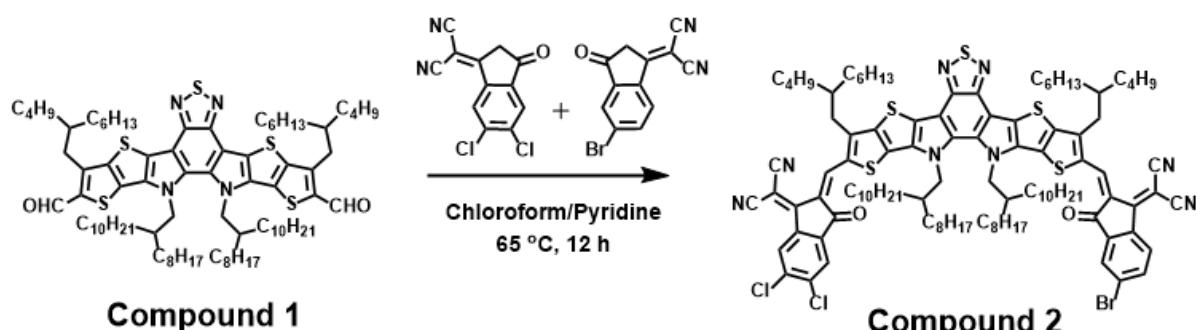
^d Department of Physics and EHSRC, University of Ulsan, Ulsan 44610, Republic of Korea

^e Department of Materials Engineering and Convergence Technology and ERI, Gyeongsang National University, Jinju 52828, Republic of Korea

Experimental Section

Materials: All solvents and reagents were purchased from Sigma-Aldrich. All solvents were purified prior to uses. 2,5-Bis(trimethylstannyl)thiophene was purchased from the Solarmer Materials Inc. All the other eluents and materials were purchased from Sigma Aldrich Co. and Tokyo Chemical Industry Co. 3,9-Bis(2-butyloctyl)-12,13-bis(2-octyldodecyl)-12,13-dihydro-[1,2,5]thiadiazolo[3,4-e]thieno[2",3":4',5']thieno[2',3':4,5]pyrrolo[3,2-g]thieno[2',3':4,5]thieno[3,2-b]indole-2,10-dicarbaldehyde and compound 3 were synthesized using similar approach of previous literature.¹⁻⁵ 2,9-Bis(3-((3-(dimethylamino)propyl)amino)propyl)anthra[2,1,9-*def*:6,5,10-*d'e'f'*]diisoquinoline-1,3,8,10(2*H*,9*H*)-tetraone (PDINN) was synthesized by following the method described in the previous literature.⁶

(1) *Synthesis of 2-((Z)-2-((3,9-bis(2-butylOctyl)-10-((Z)-5,6-dichloro-1-(dicyanomethylene)-3-oxo-1,3-dihydro-2H-inden-2-ylidene)methyl)-12,13-bis(2-octyldodecyl)-12,13-dihydro-[1,2,5]thiadiazolo[3,4-e]thieno[2'',3'':4',5']thieno[2',3':4,5]pyrrolo[3,2-g]thieno[2',3':4,5]thieno[3,2-b]indol-2-yl)methylene)-5-bromo-3-oxo-2,3-dihydro-1H-inden-1-ylidene)malononitrile (Compound 2)*



Scheme S1. Synthetic scheme for 2-((Z)-2-((3,9-bis(2-butylOctyl)-10-((Z)-5,6-dichloro-1-(dicyanomethylene)-3-oxo-1,3-dihydro-2H-inden-2-ylidene)methyl)-12,13-bis(2-octyldodecyl)-12,13-dihydro-[1,2,5]thiadiazolo[3,4-e]thieno[2'',3'':4',5']thieno[2',3':4,5]pyrrolo[3,2-g]thieno[2',3':4,5]thieno[3,2-b]indol-2-yl)methylene)-5-bromo-3-oxo-2,3-dihydro-1H-inden-1-ylidene)malononitrile (**Compound 2**).

INCN-Br-in (492 mg, 1.8 mmol), INCN-Cl (470 mg, 1.8 mmol), and 3,9-bis(2-butylOctyl)-12,13-bis(2-octyldodecyl)-12,13-dihydro-[1,2,5]thiadiazolo[3,4-e]thieno[2'',3'':4',5']thieno[2',3':4,5]pyrrolo[3,2-g]thieno[2',3':4,5]thieno[3,2-b]indole-2,10-dicarbaldehyde (compound 1, 1000 mg, 0.72 mmol) were added to a solvent mixture of chloroform (100 mL) and pyridine (4 mL) (**Scheme S1**). The reaction was placed in an oil bath at 65°C and stirred overnight. After the reaction, residual solvents were removed at low pressure (< 300 mbar), and the product was purified by silica-gel column chromatography

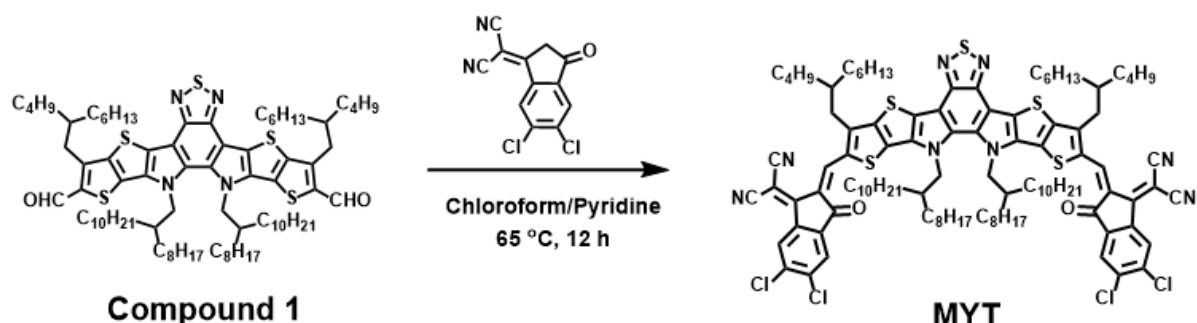
using hexane/dichloromethane (1:1) as eluent to yield compound 2 as a black solid (380 mg, 28%).

¹H NMR (300 MHz, CDCl₃) δ 9.12 (d, J = 3.3 Hz, 2H), 8.7 (s, 1H), 8.51(d, J = 8.5 Hz, 1H), 8.00 (d, J = 1.9 Hz, 1H), 7.93 (s, 1H), 7.81 (dd, J = 8.4, 1.9 Hz, 1H), 4.81 (d, J = 7.8 Hz, 4H), 3.12 (d, J = 7.4 Hz, 4H), 2.15 (t, J = 5.3 Hz, 2H), 2.06 (t, J = 5.3 Hz, 2H), 1.47 – 1.08 (m, 60H), 1.08 – 0.90 (m, 36H), 0.88 – 0.76 (m, 24H).

¹³C NMR (125 MHz, CDCl₃) δ 186.85, 186.04, 160.01, 158.77, 153.79, 153.28, 147.70, 147.67, 145.50, 145.40, 139.48, 139.14, 138.78, 138.55, 138.32, 137.78, 137.62, 136.46, 136.09, 135.90, 135.85, 134.57, 134.53, 134.44, 134.20, 131.40, 130.91, 129.51, 126.86, 126.72, 126.32, 124.90, 120.28, 119.89, 115.65, 115.45, 115.09, 114.79, 113.75, 113.56, 68.80, 68.55, 56.04, 40.06, 39.42, 34.66, 33.69, 33.41, 32.05, 32.01, 31.97, 30.84, 29.97, 29.94, 29.79, 29.73, 29.60, 29.55, 29.50, 29.46, 29.38, 28.94, 26.69, 25.94, 25.90, 23.11, 22.83, 22.78, 14.25, 14.22, 14.18.

MS (MALDI-TOF) m/z: [M + H]⁺ calculated for C₁₀₈H₁₃₉BrCl₂N₈O₂S₅, 1891.82, found: 1892.50.

(2) Synthesis of MYT



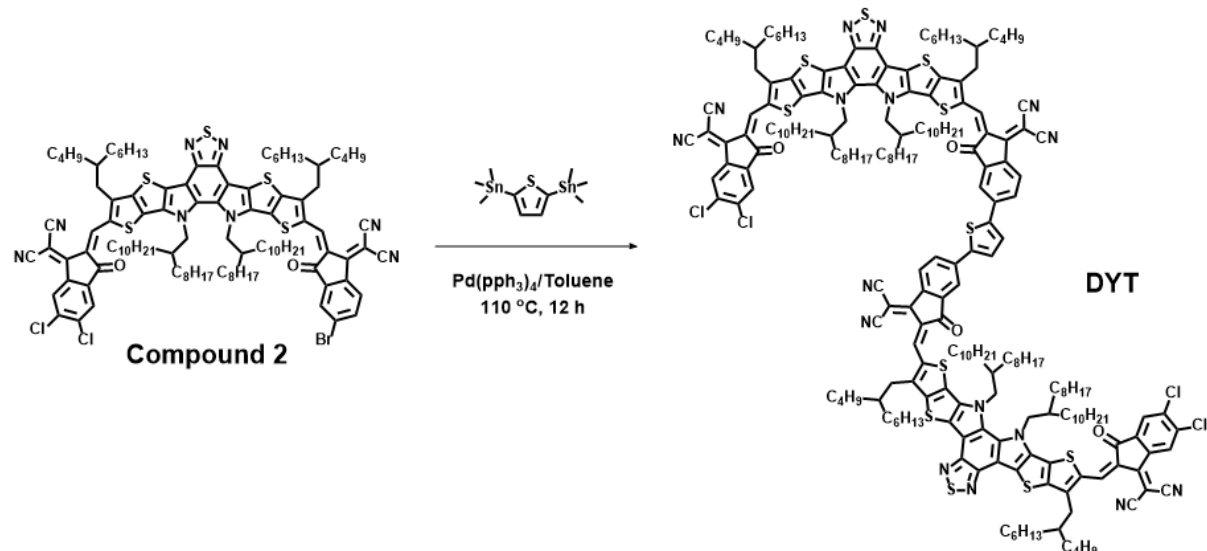
Scheme S2. Synthetic scheme for MYT.

INCN-2Cl (470 mg, 1.8 mmol) and compound 1 (500 mg, 0.36 mmol) were added to a solvent mixture of chloroform (50 mL) and pyridine (2 mL) (**Scheme S2**). The mixture was reacted in an oil bath at 65°C during overnight. After removing residual solvents at low pressure (< 300 mbar) by a rotary evaporator, the product was purified by a silica-gel column chromatography using hexane/dichloromethane (3:2) as eluent. The final MYT product had a reaction yield of 80% (550 mg).

¹H NMR (300 MHz, CDCl₃) δ 9.10 (s, 2H), 8.73 (s, 2H), 7.92 (s, 2H), 4.82 (d, J = 7.8 Hz, 4H), 3.10 (d, J = 7.4 Hz, 4H), 2.16 (t, J = 6.3 Hz, 2H), 2.05 (t, J = 5.3 Hz, 2H), 1.53 – 1.09 (m, 60H), 1.09 – 0.90 (m, 36H), 0.88 – 0.77 (m, 24H).

MS (MALDI-TOF) m/z: [M + H]⁺ calcd for C₁₀₈H₁₃₈Cl₄N₈O₂S₅, 1881.83, found: 1881.25.

(3) Synthesis of DYT



Scheme S3. Synthetic scheme for DYT.

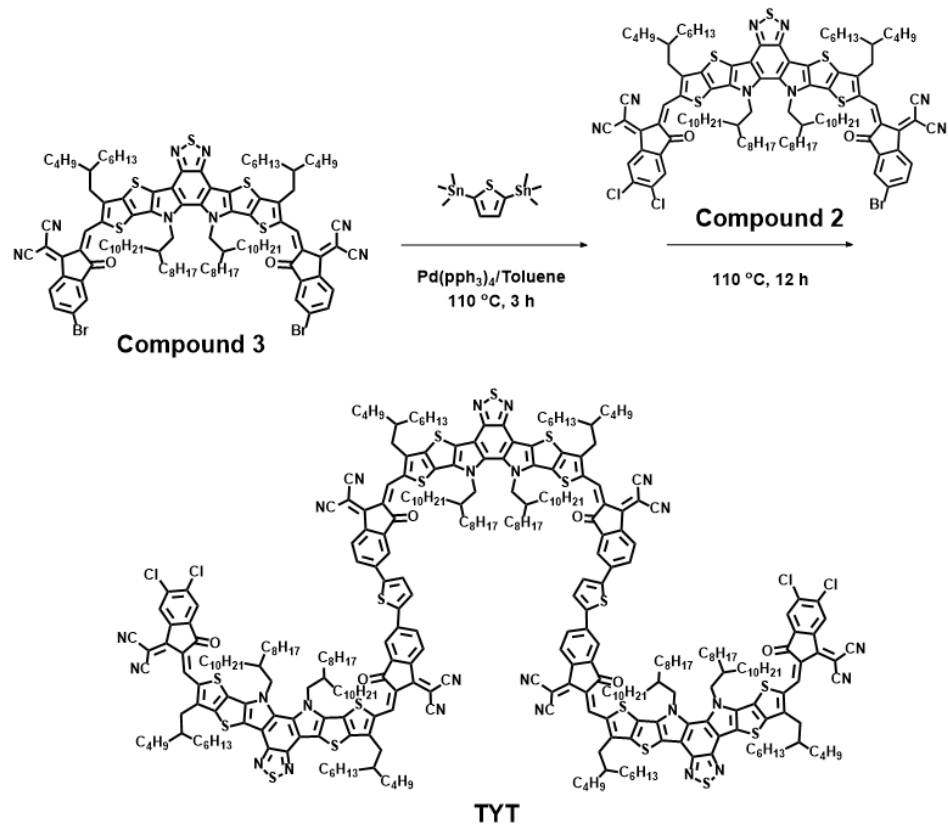
Compound 2 (380 mg, 0.2 mmol), 2,5-bis(trimethylstannyl)thiophene (33 mg, 0.08 mmol), and Pd(PPh₃)₄ (4.6 mg, 0.004 mmol) were combined in a 100 mL two-necked flask (**Scheme S3**). Anhydrous toluene (50 mL) was added under the argon atmosphere. The mixture was

reacted for 12 h at 110 °C. After the reaction, residual solvents were removed at low pressure (< 300 mbar), and the product was purified by silica-gel column chromatography using hexane/chloroform (1:1) as eluent to yield DYT as black solid (250 mg, 67%).

¹H NMR (300 MHz, CDCl₃) δ 9.12 (d, J = 13.0 Hz, 4H), 8.77 (d, J = 9.8 Hz, 4H), 8.09 (s, 2H), 8.03 – 7.96 (m, 2H), 7.79 (s, 2H), 7.65 (s, 2H), 4.84 (s, 8H), 3.12 (s, 8H), 2.20 (s, 4H), 2.07(s, 4H), 1.52 – 0.93 (m, 192H), 0.88 – 0.75 (m, 48H).

MS (MALDI-TOF) m/z: [M + H]⁺ calculated for C₂₂₀H₂₈₀Cl₄N₁₆O₄S₁₁, 3705.80, found: 3711.88.

(4) Synthesis of TYT



Scheme S4. Synthetic scheme of TYT.

Compound 3 (190 mg, 0.1 mmol), and 2,5-bis(trimethylstannylyl)thiophene (95 mg, 0.23 mmol), and Pd(PPh₃)₄ (5 mg, 0.004 mmol) were combined in a 100 mL two-necked flask (**Scheme S4**). Anhydrous toluene (30 mL) was added under the argon atmosphere. After stirring for 3 h at 110 °C, compound 2 (550 mg, 0.3 mmol) in anhydrous toluene (20 ml) was added to the reaction mixture. The mixture was reacted for 10 h at 110 °C. After removing residual solvents at low pressure (< 300 mbar) by a rotary evaporator, the product was purified by silica-gel column chromatography using chloroform as an eluent to give TYT as black solid (240 mg, 45%).

¹H NMR (300 MHz, CDCl₃) δ 9.28 – 8.59 (m, 12H), 8.25 – 7.80 (m, 8H), 7.75 – 7.44 (m, 6H), 4.92 (m, 12H), 3.19 (s, 4H), 2.72 (s, 4H), 2.51 – 2.05 (m, 12H), 2.02 – 1.71 (m, 4H), 1.52 – 0.95 (m, 288H), 0.94 – 0.62 (m, 72H).

MS (MALDI-TOF) m/z: [M + H]⁺ calculated for C₃₃₂H₄₂₂C₁₄N₂₄O₆S₁₇, 5532.01, found: 5539.51.

Characterizations: Bruker Avance Drx 300 MHz and 500 MHz FT-NMR spectrometers were used to measure ¹H NMR and ¹³C NMR spectra. The chemical shifts in the spectra have units of ppm. Bruker Autoflex MALDI-ToF mass spectrometer was used to measure the molecular weights of the DSMAs. Number-average molecular weight (M_n) and dispersity (D) of the PM6 were determined by size exclusion chromatography (SEC) analyses in 1,2,4-trichlorobenzene at 150 °C, calibrated with polystyrene standards. A UV-1800 spectrophotometer was used for the UV–Vis absorption spectra. The differential scanning calorimetry (DSC) profiles were obtained by TA Instruments DSC 25 with heating rates of 5 °C min⁻¹ from 20 to 330 °C. Cyclic voltammetry (CV) was performed using an EG and G Parc model 273 Å potentiostat/galvanostat system in a 0.1 M tetrabutylammonium perchlorate solution with nitrogen degassed anhydrous acetonitrile as the supporting electrolyte, at a scan rate of 50 mV

s^{-1} . A glassy carbon electrode was used as the working electrode. A platinum wire was used as the counter electrode, and an Ag/AgCl electrode was used as the reference electrode. The redox couple ferricenium/ferrocene was used as external standard. The highest occupied molecular orbital (HOMO) and lowest unoccupied molecular orbital (LUMO) energy levels were estimated from CV: $E_{\text{HOMO}} \text{ (eV)} = -(E_{\text{onset}}^{\text{ox.}} - E_{\text{onset}}^{\text{Fc/Fc+}}) + E_{\text{HOMO}}^{\text{Fc}}$; $E_{\text{LUMO}} \text{ (eV)} = -(E_{\text{onset}}^{\text{red.}} - E_{\text{onset}}^{\text{Fc/Fc+}}) + E_{\text{HOMO}}^{\text{Fc}}$; $E_{\text{onset}}^{\text{Fc/Fc+}} = 0.44 \text{ eV}$, $E_{\text{HOMO}}^{\text{Fc}} = -4.8 \text{ eV}$. The atomic force microscopy (AFM) images were measured by NX10 from Park Systems. Grazing incidence wide-angle X-ray scattering (GIWAXS) analysis was conducted at the Pohang Accelerator Laboratory (beamline 9A, Republic of Korea), with incidence angles between $0.12 - 0.14^\circ$. The resonant soft X-ray scattering (RSoXS) experiment was performed at beamline 11.0.1.2 in the S11 Advanced Light Source (United States). Blend films for the RSoXS measurement were prepared on a 100 nm-thick, $1.0 \text{ mm} \times 1.0 \text{ mm}$ Si_3N_4 membrane supported by a 200- μm thick, $5 \text{ mm} \times 5 \text{ mm}$ silicon frame (Norcada Inc.). The optimized molecular structures were calculated by density functional theory (DFT) method with the B3LYP function and the 6-31G* basis set using a modelling software (Spartan'14).

OSC Fabrication and Characterization: The OSCs with a normal architecture (indium tin oxide (ITO)/ poly(3,4-ethylenedioxythiophene):poly(styrenesulfonate) (PEDOT:PSS)/active layer/PDINN/Ag) were prepared with the following procedures. ITO-coated glass substrates were treated by ultrasonication with deionized water, acetone, and isopropyl alcohol. Then, the ITO substrates were dried for 6 h in an oven (70°C) at an ambient pressure, and then plasma treated for 10 min. Spin-coating of the PEDOT:PSS solution (Clevios, AI4083) was performed at 3000 rpm for 30 s onto the ITO substrates, then the substrate/film was annealed in air (150°C , 15 min) before transferring into an N_2 -filled glovebox. The active layer solutions were

dissolved together in chlorobenzene with an optimized condition (donor:acceptor blend ratio = 1:1 w/w, concentration = 20 mg mL⁻¹, and 1-chloronaphthalene 0.75 vol%), and then stirred on a 90 °C plate during overnight. The solution was spin-coated onto the ITO substrates/PEDOT:PSS samples to form active layers with a thickness range of 94 – 108 nm. Then, the samples were dried with high vacuum (< 10⁻⁶ torr) for 1 h and annealed at 120 °C for 10 min. PDINN in methanol (1 mg mL⁻¹) was then spin-coated with the condition of 2500 rpm for 30 s. Finally, Ag (120 nm) was deposited under high vacuum (~10⁻⁶ Torr) in an evaporation chamber. Optical microscopy (OM) was used to measure the exact photoactive area of the mask (0.09 cm²). Keithley 2400 SMU instrument was used to measure the power conversion efficiencies (PCEs) under an Air Mass 1.5 G solar simulator (100 mW cm⁻², solar simulator: K201 LAB55, McScience), satisfying the Class AAA, ASTM Standards. K801SK302 of McScience was used as a standard silicon reference cell to calibrate the exact solar intensity. The reference cell was calibrated every 3 months, and the most recent calibration date was Dec. 7, 2022. K3100 IQX, McScience Inc. instrument was used to analyze the external quantum efficiency (EQE) spectra, equipped with a monochromator (Newport) and an optical chopper (MC 2000 Thorlabs).

Space-Charge-Limited Current (SCLC) Mobility Measurements: Hole and electron mobilities of pristine constituents and blend films were measured by SCLC method using device structures of ITO/PEDOT:PSS/active layers/Au (hole-only) and ITO/ZnO/polymer blends/Ca/Al (electron-only). A range of voltage from 0 to 6 V was applied for the current-voltage measurements, and the results were fitted by the Mott-Gurney law.

$$J = \frac{9\epsilon_0\epsilon_r\mu_0V^2}{8L^3}$$

where J is the current density, ε_0 is the permittivity of free space ($8.85 \times 10^{-14} \text{ F cm}^{-1}$), ε_r is the relative dielectric constant of the transport medium (active layer), μ_0 is the charge carrier (hole or electron) mobility, V is the potential across the device ($V = V_{\text{applied}} - V_{\text{bi}} - V_r$, where V_{bi} is the built-in potential and V_r is the voltage drop caused by the resistance), and L is the thickness of the blend or pristine films. The hole and electron mobilities can be calculated from the slope of the $J^{1/2}$ - V curves.

Estimation of Device Lifetimes: Linear extrapolation was used to estimate the device lifetimes from the thermal- and photo-stability tests, following the methods from previous literature.^{7, 8} The data points after burn-in degradation (200 – 1000 h) were used for the extrapolation using a linear-fit function. The fitted graphs were matched well with the data points.

V_{loss} Measurement and Estimation: Fourier-transform photocurrent spectroscopy (FTPS)-EQE was measured in an in-house built FTPS setup, which consisted of an INVENIO-R Fourier-transform infrared spectrometer, equipped with quartz beam splitter. The photocurrent produced by the solar cell under illumination was amplified using a SR570 low-noise preamplifier from Stanford Research Systems and fed back into the external detector port of the FTIR. Electroluminescence (EL) signals passed through the integral sphere and were collected by using MAYA2000 PRO spectrophotometer from Ocean optics. The photovoltaic bandgap energy (E_g^{PV}) of each blend was determined from the derivatives of the EQE spectra, which is generally utilized method in previous work.^{9, 10}

Based on the detailed balance theory and reciprocity in solar cells,^{9, 10} the V_{loss} of solar cells is decomposed into three terms:

$$V_{\text{loss}} = \Delta E_1 + \Delta E_2 + \Delta E_3 = (E_g^{\text{PV}}/q - V_{\text{oc}}^{\text{SQ}}) + (V_{\text{oc}}^{\text{SQ}} - V_{\text{oc}}^{\text{Rad}}) + (V_{\text{oc}}^{\text{Rad}} - V_{\text{oc}}^{\text{PV}})$$

The first V_{loss} term (ΔE_1) is defined by Shockley-Queisser (SQ) limit,¹⁰ which is the maximal voltage for V_{oc} . $V_{\text{oc}}^{\text{SQ}}$ is calculated by

$$V_{\text{oc}}^{\text{SQ}} = \frac{k_B T}{q} \ln \left[\frac{q \int_{E_g}^{\infty} \phi_{AM\ 1.5G}(E) dE}{q \int_{E_g}^{\infty} \phi_{BB}(E) dE} + 1 \right]$$

where k_B is Boltzmann constant, T is temperature of solar cell, q is electric charge, $\Phi_{\text{AM}\ 1.5G}$ is irradiance of standard solar simulator, and $\phi_{BB}(E)$ is the blackbody spectrum of semiconductor, given by:¹¹

$$\phi_{BB}(E) = \frac{2\pi E^2}{h^3 c^2} \exp \left[-\frac{E}{k_B T} \right]$$

where h is Planck constant and c is speed of light.

The second V_{loss} term (ΔE_2) is the offset between the SQ limited voltage and open-circuit voltage in the radiative limit ($V_{\text{oc}}^{\text{Rad}}$), where only radiative recombination of electron-hole pairs is allowed. Since the $V_{\text{oc}}^{\text{Rad}}$ is assumed in practical case, the equation going to be:

$$V_{\text{oc}}^{\text{Rad}} = \frac{k_B T}{q} \ln \left[\frac{J_{\text{sc}}}{q \int_{E_g}^{\infty} Q_{\text{eqe}}(E) \cdot \phi_{BB}(E) dE} + 1 \right]$$

where J_{sc} is short-circuit current density of solar cells and $Q_{\text{eqe}}(E)$ is the EQE obtained by the principle of detailed balance and reciprocity theorem.

The third V_{loss} term (ΔE_3) is the non-radiative loss, which is extracted by subtracting the $V_{\text{oc}}^{\text{Rad}}$ to V_{oc} of the solar cells. Alternatively, ΔV_3 also can be obtained by theoretical approach given by:

$$\Delta E_3 = -\frac{k_B T}{q} \ln(EQE_{\text{EL}}).$$

Photostability test of the OSCs: The OSCs' photostability was examined under 1-sun illumination (100 mW cm^{-2}) in an N_2 -filled glovebox. A Xenon lamp (Xe-55, McScience) was employed for irradiation without blocking ultraviolet light. A silicon solar cell (K801SK302, McScience) served as a standard reference for calibrating the precise solar intensity. The photostability test was conducted at an ambient temperature, and the surface temperatures of the devices reached $60 - 70^\circ\text{C}$ when measured using a pyrometer. The OSCs, featuring a complete device structure (ITO/PEDOT:PSS/active layer/PNDITF3N-Br/Ag) without encapsulation, were illuminated for 1000 h and subsequently measured using the same instrument and method as described above. Each data point represents the average of three independent devices.

Estimation of glass-transition temperature: UV-vis spectroscopy was used to determine the glass transition temperature (T_g). The absorption spectra of DSMA films were measured with increasing thermal annealing temperatures from 20 to 200°C . Then, the deviation metric (DM_T) of the each absorption spectra was calculated, following the method from Samuel E. Root et al.¹²

$$\text{DM}_T \equiv \sum_{\lambda_{\min}}^{\lambda_{\max}} [\text{I}_{RT}(\lambda) - \text{I}_T(\lambda)]^2$$

where λ is the wavelength, λ_{\max} and λ_{\min} are the upper and lower bounds of the optical sweep, respectively, $\text{I}_{RT}(\lambda)$ and $\text{I}_T(\lambda)$ are the normalized absorption intensities of the as-cast (room temperature) and annealed films, respectively. Then, T_g s were determined to points where the two interpolated lines in low- and high-temperature regions intersect.

Estimation of diffusion coefficient at 85°C (D_{85}): The D_{85} s of the acceptor constituents (in blend films with PM6) were estimated following the method (*i.e.*, Ghasemi–O’Connor–Ade

framework) in previous literature.¹³ In the study, Ghasemi *et al.* estimated T_{gS} (or cold-crystallization temperatures, T_{ccS}) of various acceptor constituents (*i.e.*, EH-IDTBR, di-PDI, IT-M, IEICO-Cl, ITIC-4Cl, and Y6) by measuring D_{MT} of UV-absorbances or DSC of pristine acceptor materials. They also monitored D_{85S} of the acceptor constituents in blend films with specific donors (*i.e.*, P3HT, FTAZ/HTAZ, PTB7-Th, and PBDB-T/PBDB-T2F (PM6)) at 85°C by obtaining time-of-flight secondary ion mass spectrometry (ToF-SIMS) profiles. They found that D_{85S} of the acceptors (in the blend films with given donors) had strong correlation with their T_{gS} , showing an exponential decrease in the D_{85} as the T_g increased ($D_{85}(\text{cm}^2\text{s}^{-1}) = a \times e^{b \times T_g(\text{K})}$); the coefficients (a and b) in the exponential equations were determined depending on the given donors. When PM6 or PBDB-T donor was used, the D_{85S} of the acceptor components in the blend with donors were determined as $D_{85}(\text{cm}^2\text{s}^{-1}) = 1.2 \times 10^7 \times e^{-0.15 \times T_g(\text{K})}$.

Time-of-flight secondary ion mass spectrometry (ToF-SIMS) measurement: The ToF-SIMS experiments were conducted using a TOF-SIMS5 instrument from ION-TOF GmbH incorporation. Bi3+ ions were used as the primary ion source (energy = 30 keV), and Ar-cluster functioned as the sputtering source (energy = 2.5 keV) during the ToF-SIMS experiments. The sample fabrication process for the TOF-SIMS analysis involved several steps to create acceptor-donor bilayers on silicon (Si) substrates: 1) dissolution of donor and acceptor materials in chlorobenzene (CB) at concentrations of 12.5 mg mL⁻¹ (donor) and 30 mg mL⁻¹ (acceptor). 2) spin-casting of acceptor materials (MYT, DYT, and TYT) onto silicon (Si) substrates to form thin films. 3) spin-casting of donor polymer (PM6) onto polystyrene sulfonate (PSS)-coated glass substrates, resulting in a 40 nm thick film. 4) floating and careful detachment of PM6 thin-films from PSS-coated glass substrates in water. 5) transfer and

assembly of PM6 thin-films onto acceptor material surfaces, yielding acceptor-donor bilayers.

Estimation of D_{120} from ToF-SIMS profiles: The D_{120} s of the acceptors within the polymer were extracted using the concentration-independent 1D solution of Fick's 2_{nd} law, following methodologies described in previously published literatures.^{13, 14}

$$C(x, t_a) = C_0 \times \operatorname{erfc} \left(\frac{x - x_0}{2\sqrt{Dt_a}} \right)$$

In the given equation, $C(x, t_a)$, represents the concentration of a particular component as a function of annealing time (t_a) and position (x) within a sample. C_0 represents the fixed concentration near the PM6/acceptors interface at location x_0 . The variable D represents the concentration-independent diffusion coefficient, which characterizes the rate at which the acceptor molecules diffuse through the donor matrix. In the composition-sputtering time profiles obtained from ToF-SIMS experiments, the sputtering rate of PM6 was used to convert sputtering time to thickness. The diffusion rate of the PM6 was calculated after measuring the film thickness, by dividing the film thickness by the sputtering time (in this study, the sputtering rate of PM6 was determined to be 1.68 nm s^{-1}).

Supplementary Figures & Tables

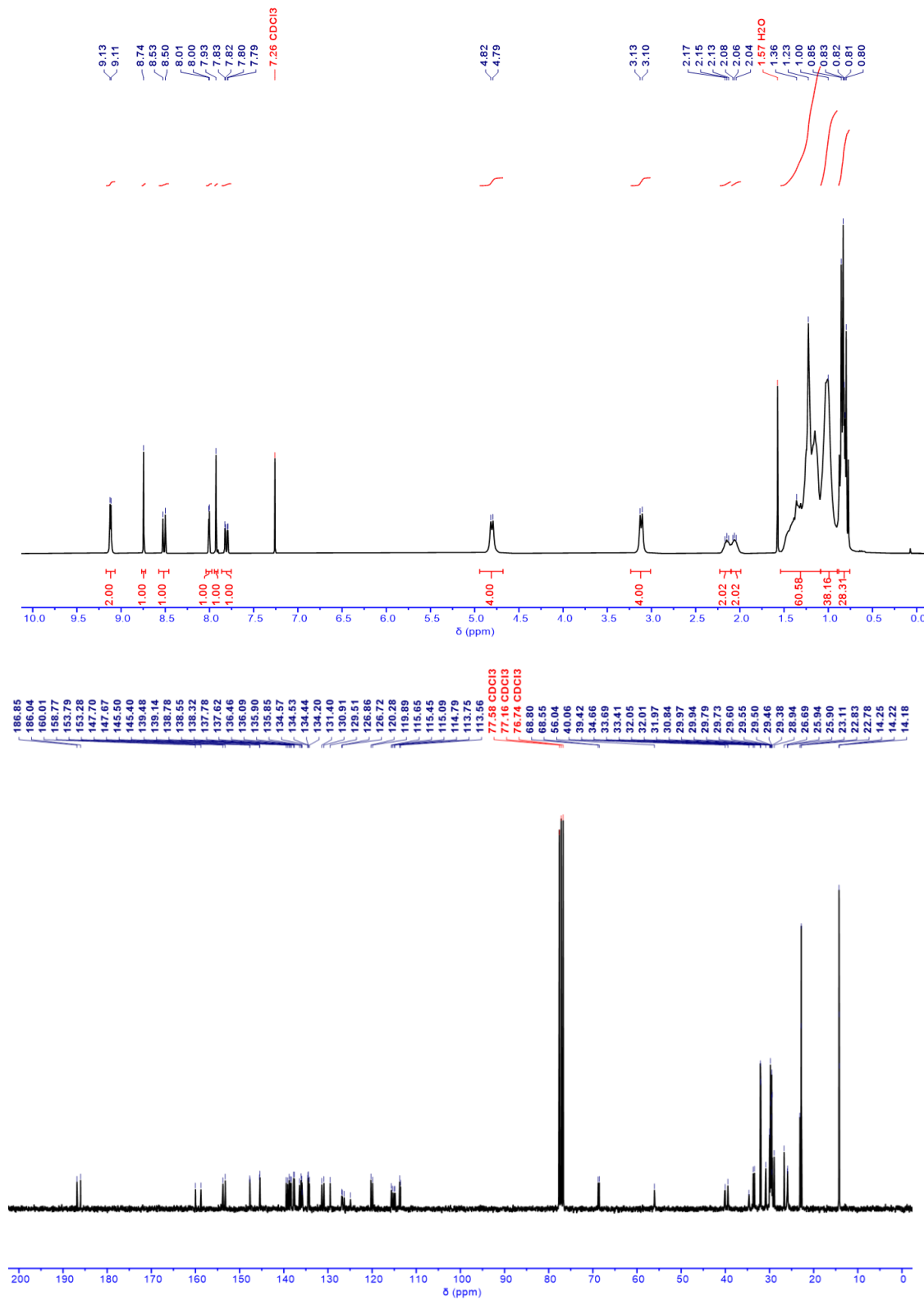


Fig. S1. ^1H -NMR and ^{13}C -NMR spectra of Compound 2 in CDCl_3 .

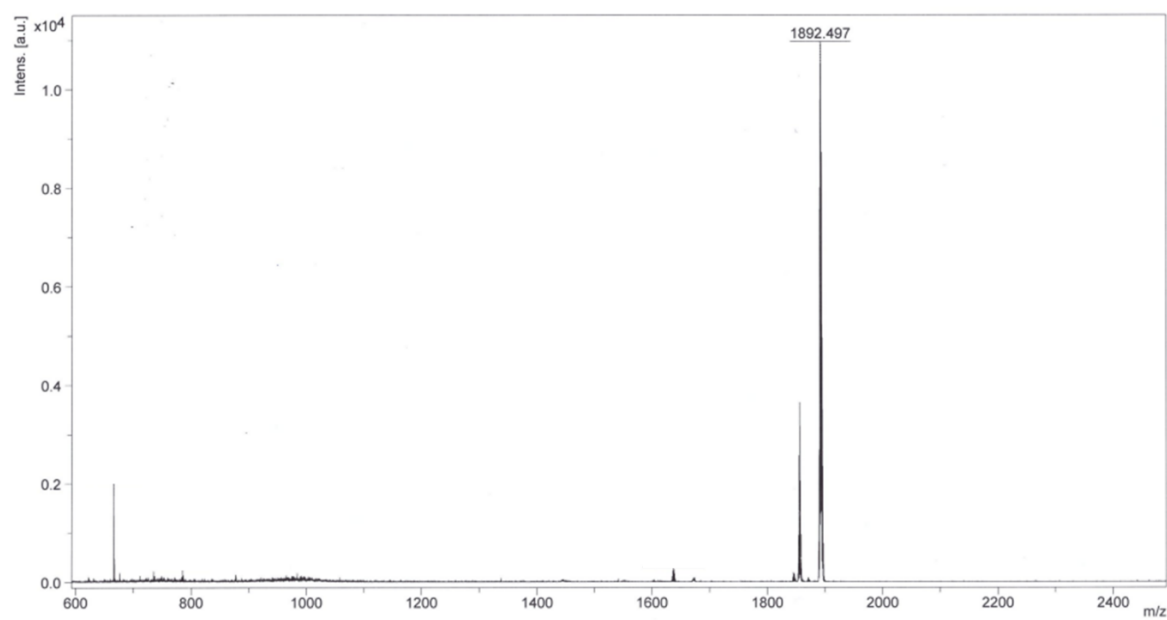


Fig. S2. MALDI-ToF spectrum of Compound 2.

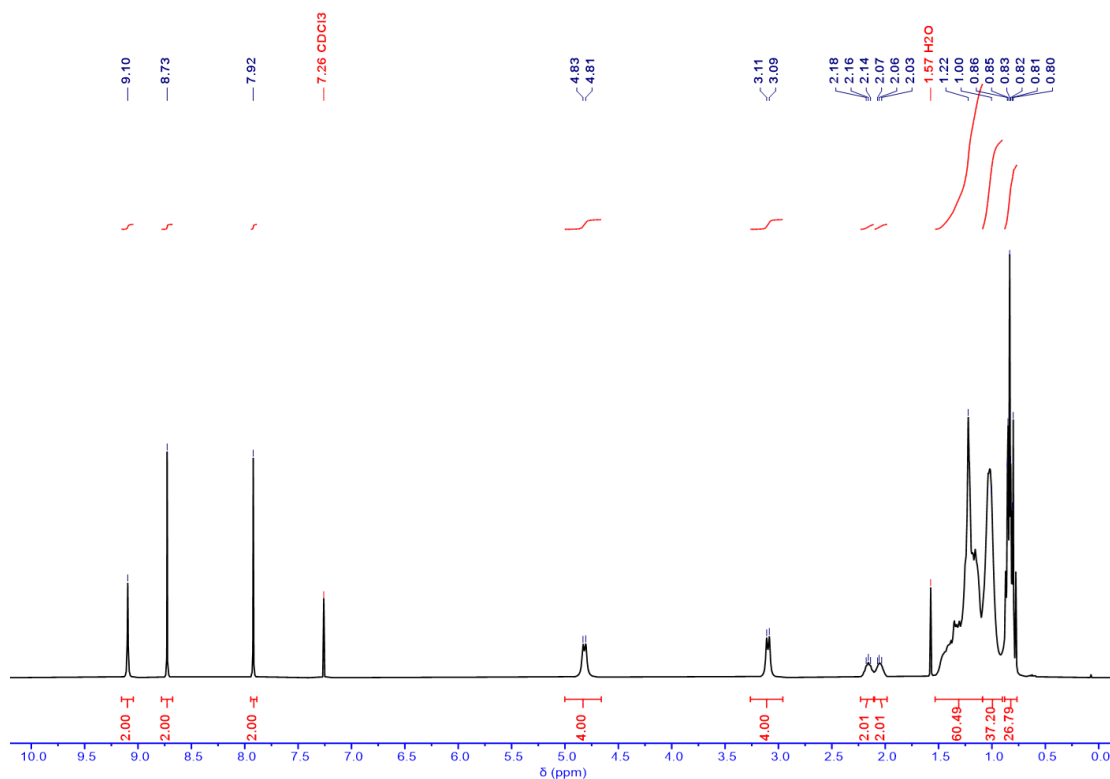


Fig. S3. ^1H -NMR spectrum of MYT in CDCl_3 .

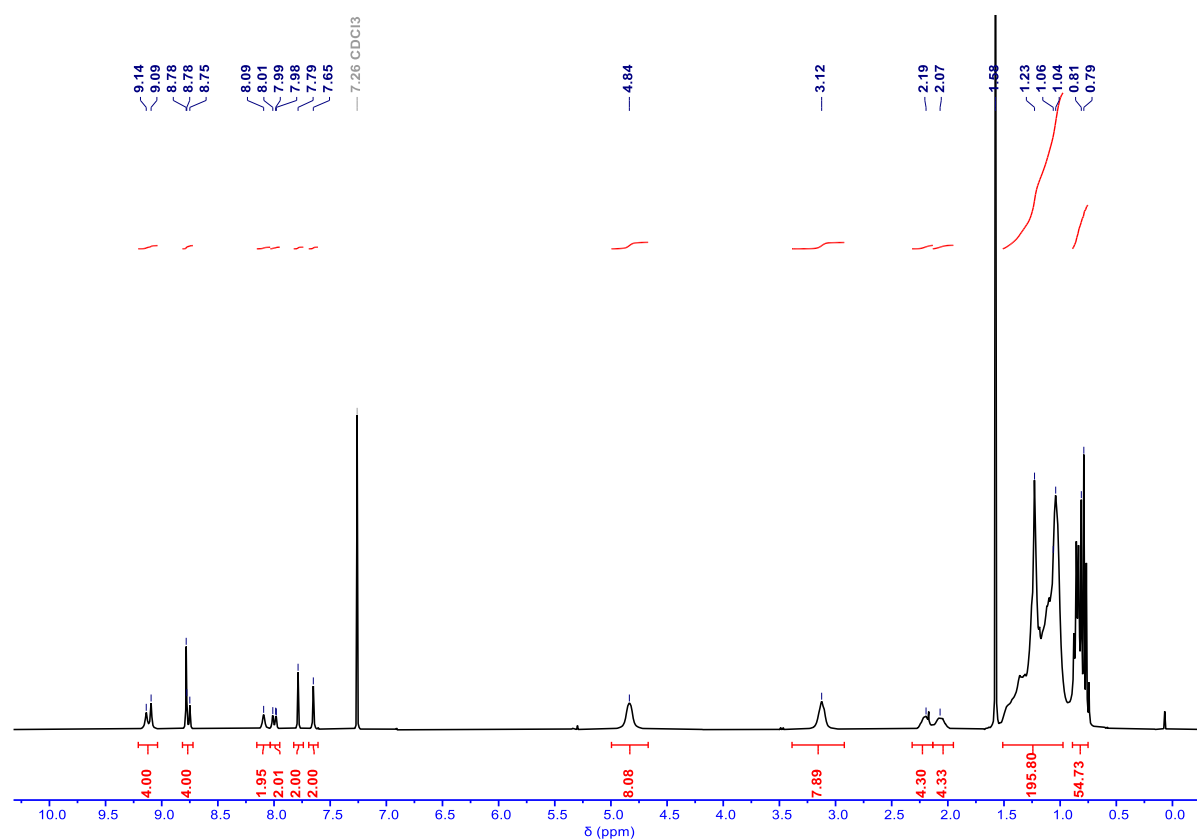


Fig. S4. ^1H -NMR spectrum of DYT in CDCl_3 .

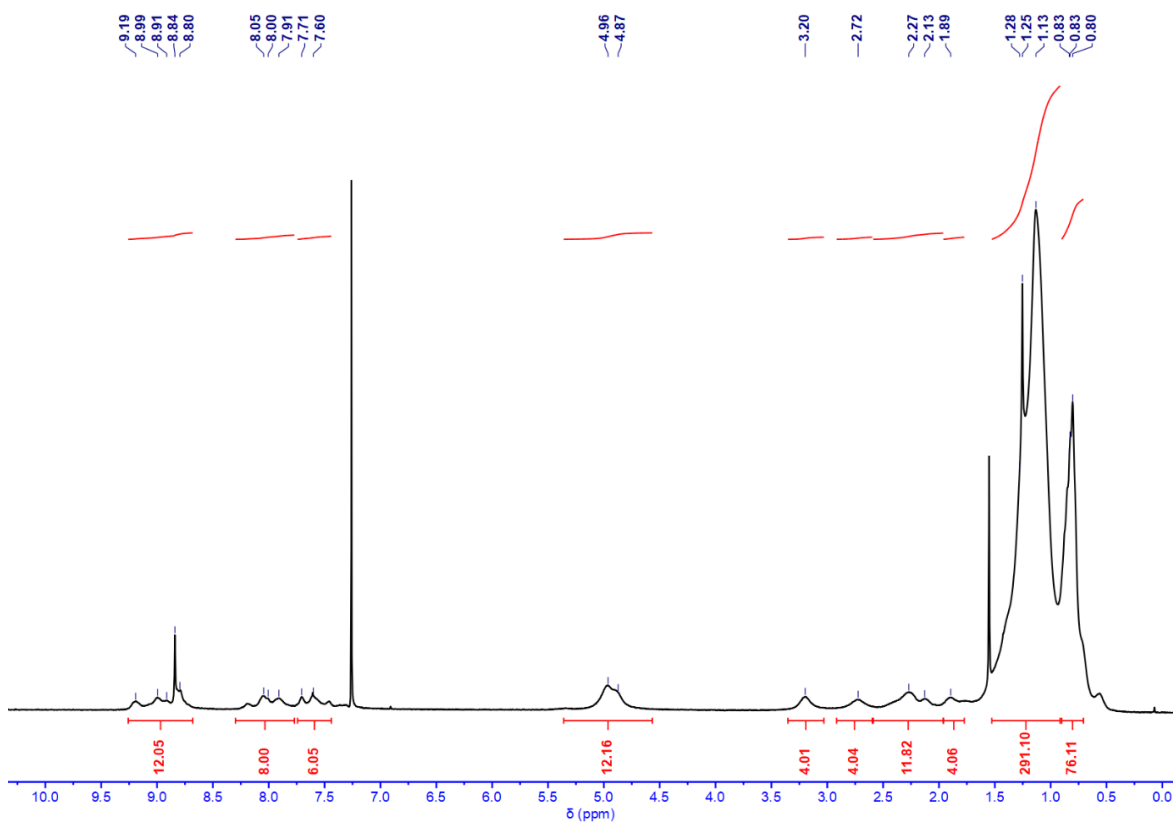


Fig. S5. ^1H -NMR spectrum of TYT in CDCl_3 .

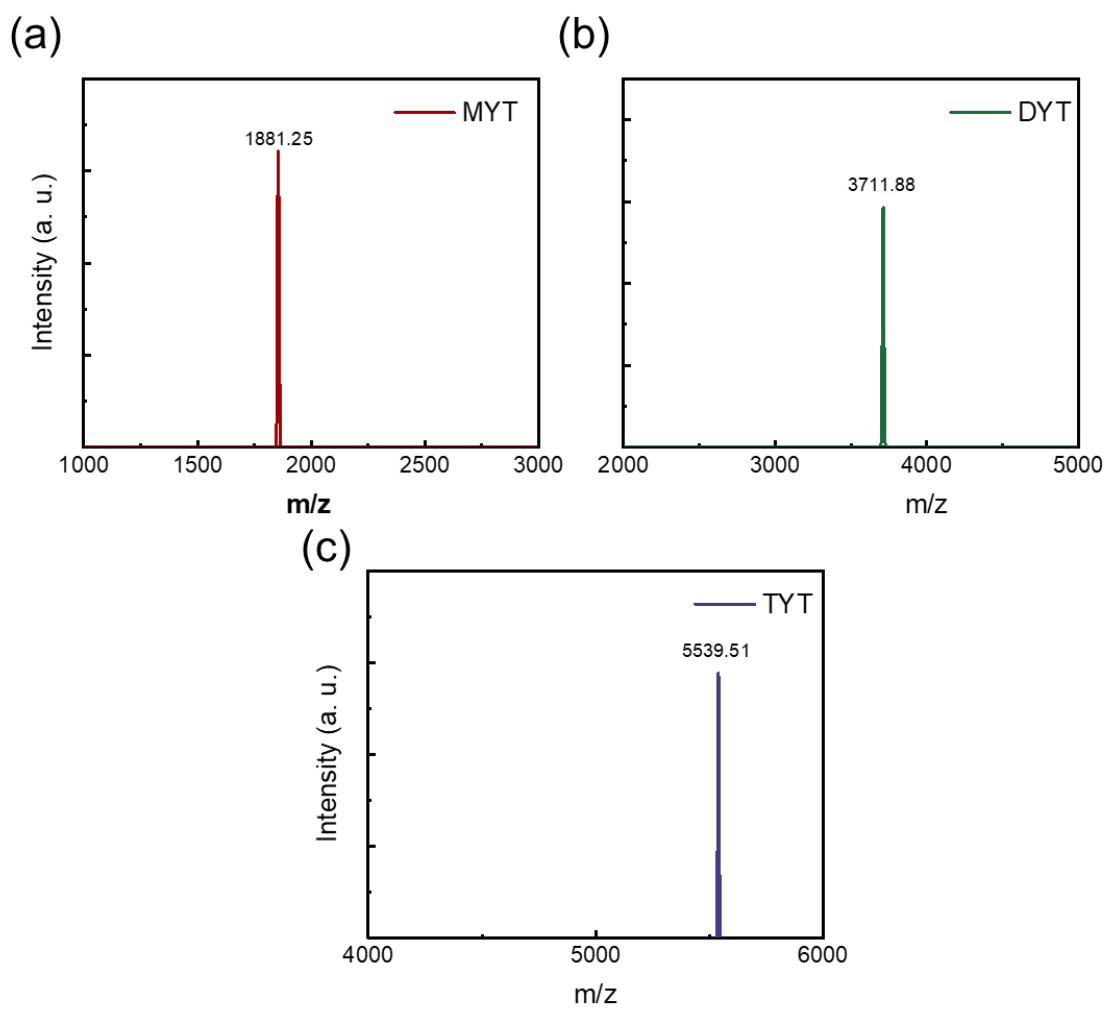


Fig. S6. MALDI-ToF spectra of the acceptors; (a) MYT, (b) DYT, and (c) TYT.

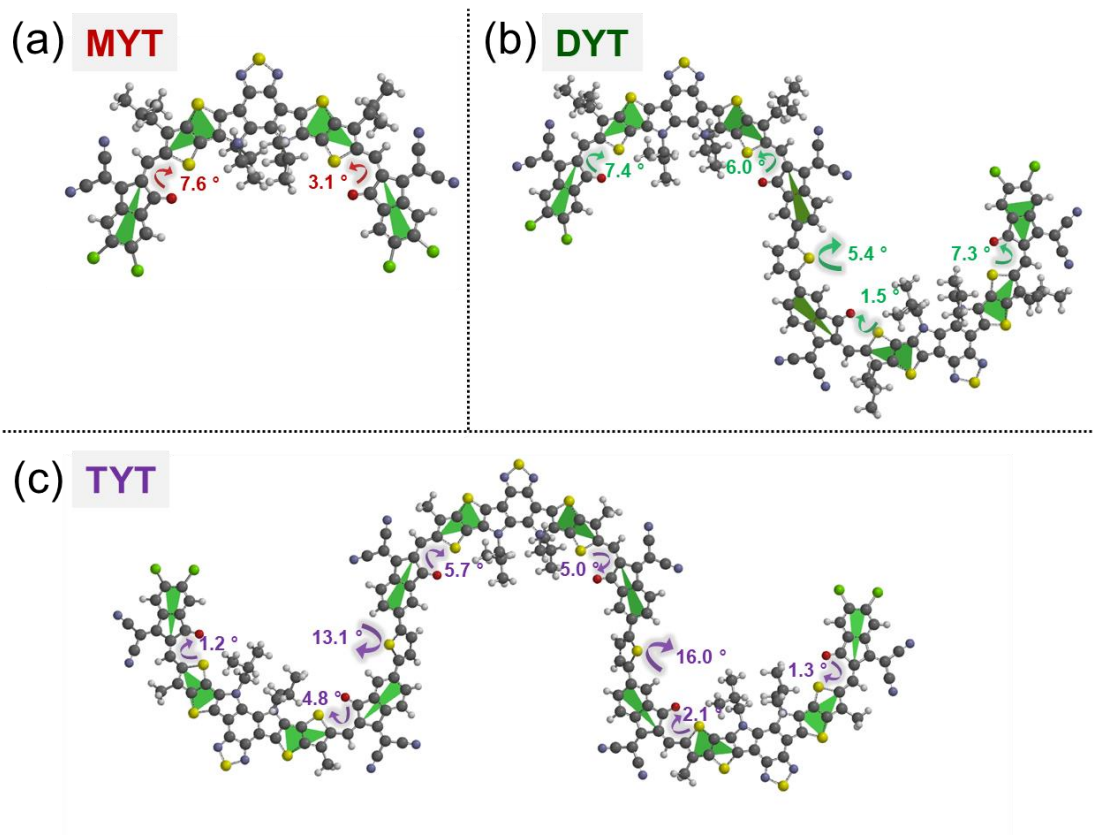


Fig. S7. Optimized molecular conformations and dihedral angles of the acceptors obtained from DFT simulations.

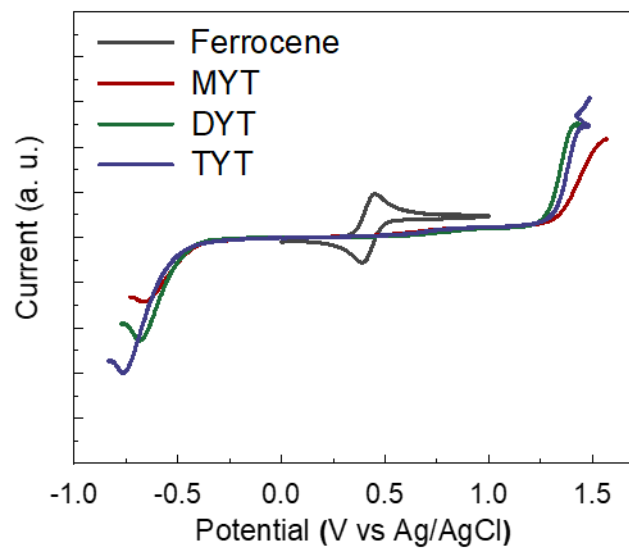


Fig. S8. Cyclic voltammogram of the acceptors.

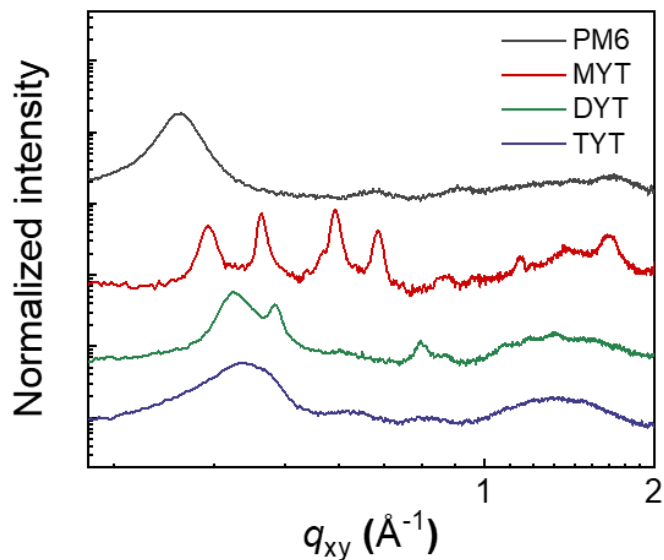


Fig. S9. GIWAXS line-cut profiles of pristine constituents in the IP direction.

Table S1. d -spacings for the (010) peaks of the pristine acceptor constituents

| Material | d -spacing (Å) |
|----------|------------------|
| MYT | 3.81 |
| DYT | 3.95 |
| TYT | 4.01 |

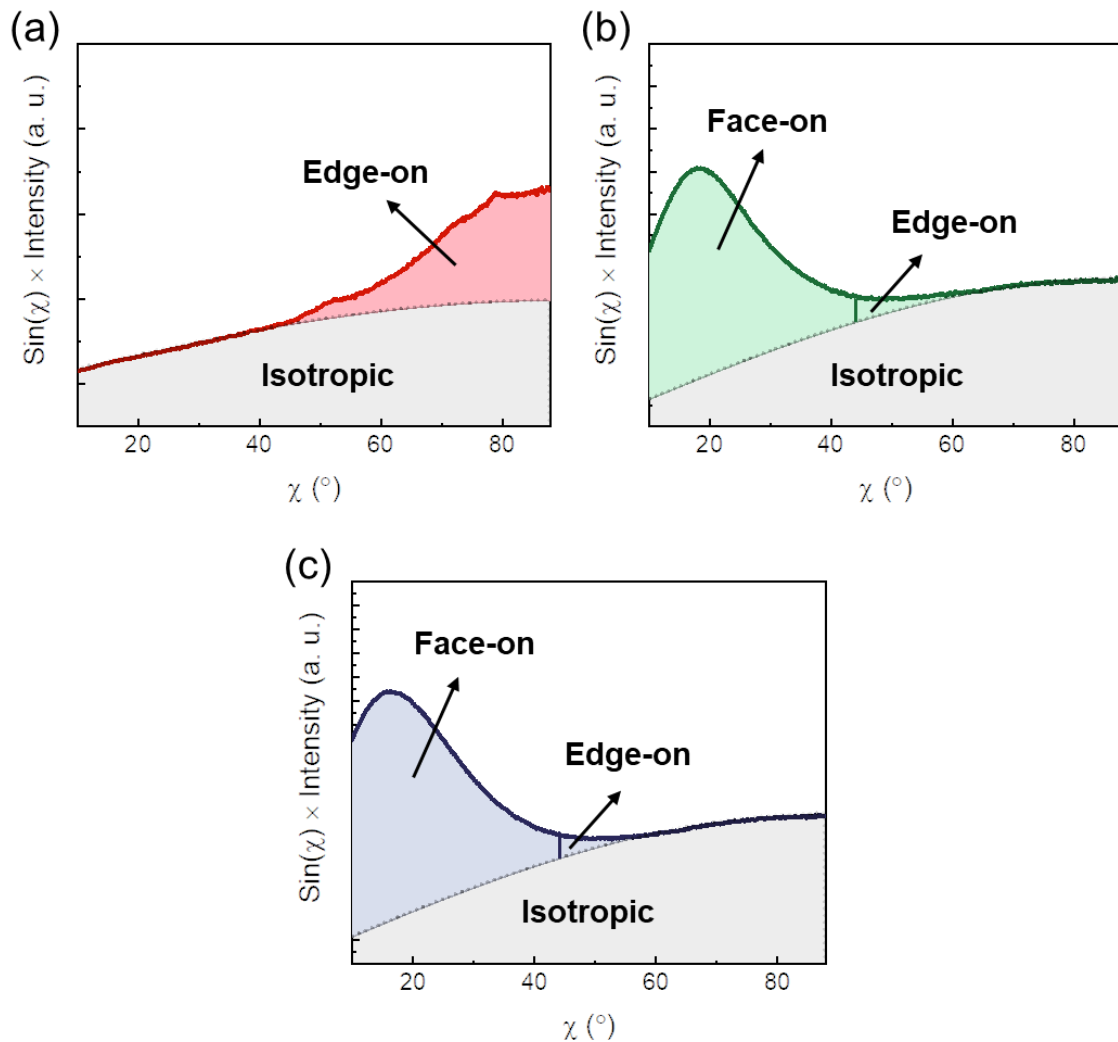


Fig. S10. Pole figures for (a) MYT, (b) DYT, and (c) TYT, acquired at (010) scattering peaks using GIWAXS linecut profiles.

Table S2. SCLC mobilities for the pristine films.

| Material | μ_h ($\text{cm}^2 \text{V}^{-1} \text{s}^{-1}$) | μ_e ($\text{cm}^2 \text{V}^{-1} \text{s}^{-1}$) |
|------------|---|---|
| PM6 | $(4.4 \pm 0.3) \times 10^{-4}$ | — |
| MYT | — | $(9.4 \pm 0.4) \times 10^{-5}$ |
| DYT | — | $(1.8 \pm 0.2) \times 10^{-4}$ |
| TYT | — | $(2.2 \pm 0.3) \times 10^{-4}$ |

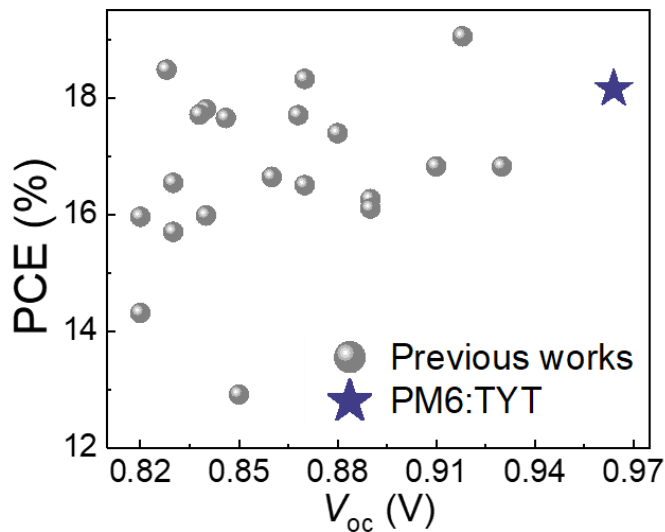


Fig. S11. PCE vs. V_{oc} plots of the reported high-performance OSCs.

Table S3. V_{oc} and PCE values of the high-performance OSCs in previous works and this work.

| System | V_{oc} (V) | PCE (%) | References |
|------------------------|--------------|---------|---------------|
| PM6:Y6 | 0.83 | 15.7 | ¹⁵ |
| PBDB-TF:BTP-4Cl | 0.867 | 16.5 | ¹⁶ |
| PM6:N3 | 0.837 | 15.98 | ¹⁷ |
| PM6:N4 | 0.819 | 14.31 | ¹⁷ |
| PM6:N-C11 | 0.852 | 12.91 | ¹⁷ |
| PM6:BTP-eC9 | 0.839 | 17.8 | ¹⁸ |
| PM6:AQx-1 | 0.89 | 13.31 | ¹⁹ |
| PM6:AQx-2 | 0.86 | 16.64 | ¹⁹ |
| PM6:BTP-ClBr | 0.906 | 16.82 | ²⁰ |
| PM6:CH1007 | 0.82 | 15.96 | ²¹ |
| PM6:Y11 | 0.833 | 16.54 | ²² |
| PM6:L8-BO | 0.87 | 18.32 | ²³ |
| PM6:L8-HD | 0.88 | 17.39 | ²³ |
| PM6:L8-OD | 0.89 | 16.26 | ²³ |
| PM6:L8-BO-F | 0.934 | 16.82 | ²⁴ |
| PM6:Y6-1O | 0.89 | 16.1 | ²⁵ |
| PM6:mBzS-4F | 0.804 | 17.02 | ²⁶ |
| PM6:EHBzS-4F | 0.825 | 15.94 | ²⁶ |

| | | | |
|--------------------------|--------------|--------------|------------------|
| PTzBI-dF:Y6 | 0.85 | 16.8 | ²⁷ |
| SZ5:BPT-4F | 0.853 | 16.5 | ²⁸ |
| SZ5:BPS-4F | 0.822 | 16.1 | ²⁸ |
| PBQ10:Y6 | 0.85 | 16.34 | ²⁹ |
| D18:Y6-Se | 0.839 | 17.7 | ³⁰ |
| PT2:Y6 | 0.83 | 16.5 | ³¹ |
| SZ4:N3 | 0.848 | 17.1 | ³² |
| PBTT-F:Y6 | 0.84 | 16.1 | ³³ |
| Pt10:Y6 | 0.81 | 16.35 | ³⁴ |
| PTQ10:Y6 | 0.87 | 16.21 | ³⁵ |
| PBNT-BDD:Y6 | 0.88 | 16.1 | ³⁶ |
| PTQ10:m-BTP-C6Ph | 0.883 | 17.7 | ³⁷ |
| PM6:M3 | 0.91 | 16.67 | ³⁸ |
| PM6:BTP-2F-ThCl | 0.869 | 17.06 | ³⁹ |
| PM6:BTP-S2 | 0.945 | 16.37 | ⁴⁰ |
| PM6:BP4T-4F | 0.839 | 17.1 | ⁴¹ |
| PM6:Y18 | 0.84 | 17.1 | ⁴² |
| PM6:BTP-S9 | 0.846 | 17.56 | ⁴³ |
| D18:N3 | 0.842 | 17.46 | ⁴⁴ |
| PBDB-T:LL3 | 0.79 | 16.82 | ⁴⁵ |
| D18:BO-4Cl | 0.86 | 17.6 | ⁴⁶ |
| PM6:A-WSSE-Cl | 0.85 | 17.51 | ⁴⁷ |
| PM6:MQ6 | 0.88 | 16.39 | ⁴⁸ |
| PBCT-2F:Y6 | 0.85 | 17.1 | ⁴⁹ |
| PNTB6-Cl:N3 | 0.857 | 17.59 | ⁵⁰ |
| PM6:BTP1O-4Cl-C12 | 0.91 | 17.1 | ⁵¹ |
| PBDB-TF:eC9 | 0.846 | 17.65 | ⁵² |
| PBQx-TF:eC9-2Cl | 0.868 | 17.7 | ⁵³ |
| D18:L8-BO | 0.918 | 19.05 | ⁵⁴ |
| D18/S9TBO-F | 0.838 | 17.71 | ⁵⁵ |
| D18/BS3TSe-4F | 0.828 | 18.48 | ⁵⁵ |
| PM6: TYT | 0.964 | 18.15 | This work |

Table S4. Photovoltaic parameters of OSCs with distinct P_D :acceptor pairs.

| Donor | Acceptor | V_{oc} (V) | J_{sc} (mA cm $^{-2}$) | FF | $PCE_{max\ avg}^a$ (%) |
|---------|----------|-----------------|------------------------------|------|---------------------------|
| D18 | MYT | 0.930 | 24.15 | 0.74 | 16.53 (16.30) |
| | DYT | 0.946 | 24.18 | 0.75 | 17.16 (16.91) |
| | TYT | 0.968 | 24.19 | 0.75 | 17.47 (17.33) |
| D18-Cl | MYT | 0.934 | 23.47 | 0.74 | 16.22 (15.98) |
| | DYT | 0.949 | 23.24 | 0.74 | 16.32 (16.10) |
| | TYT | 0.971 | 23.20 | 0.74 | 16.67 (16.37) |
| PBQx-TF | MYT | 0.896 | 25.10 | 0.75 | 16.87 (16.54) |
| | DYT | 0.928 | 24.28 | 0.75 | 16.89 (16.60) |
| | TYT | 0.950 | 24.02 | 0.75 | 17.11 (16.95) |

^aEstimated more than 5 different devices.

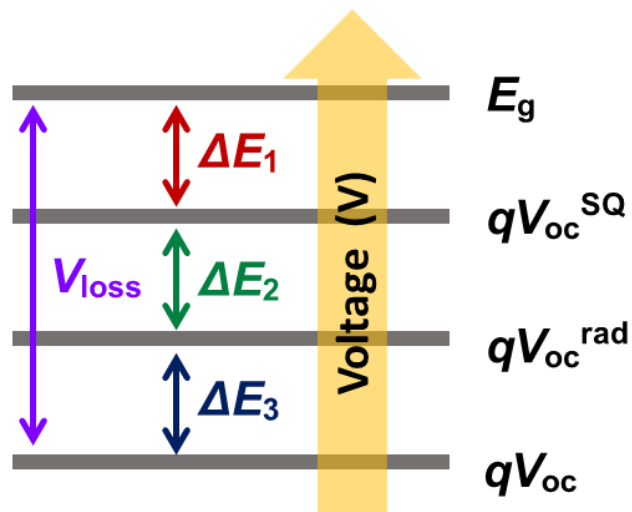


Fig. S12. Diagram describing V_{loss} .

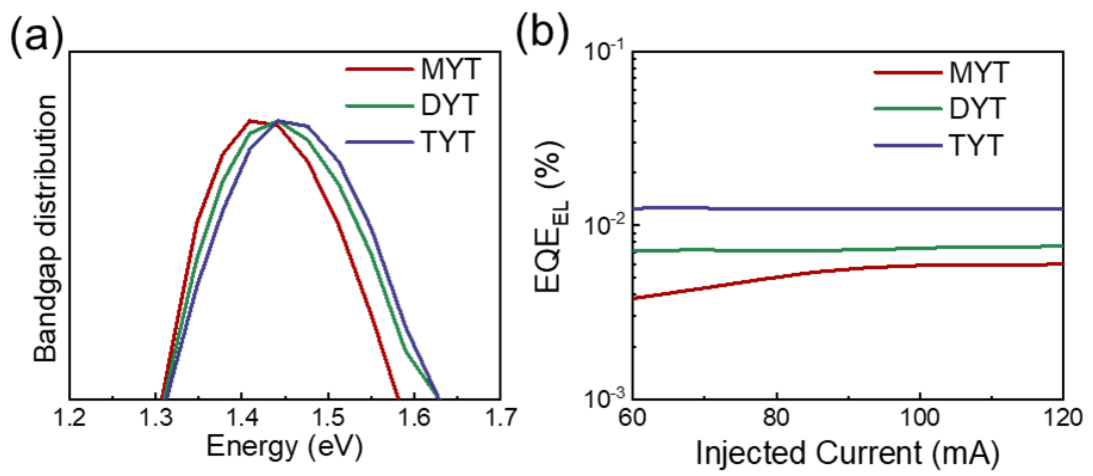


Fig. S13. (a) Bandgap distribution and (b) EQE_{EL} of the PM6:acceptor OSCs.

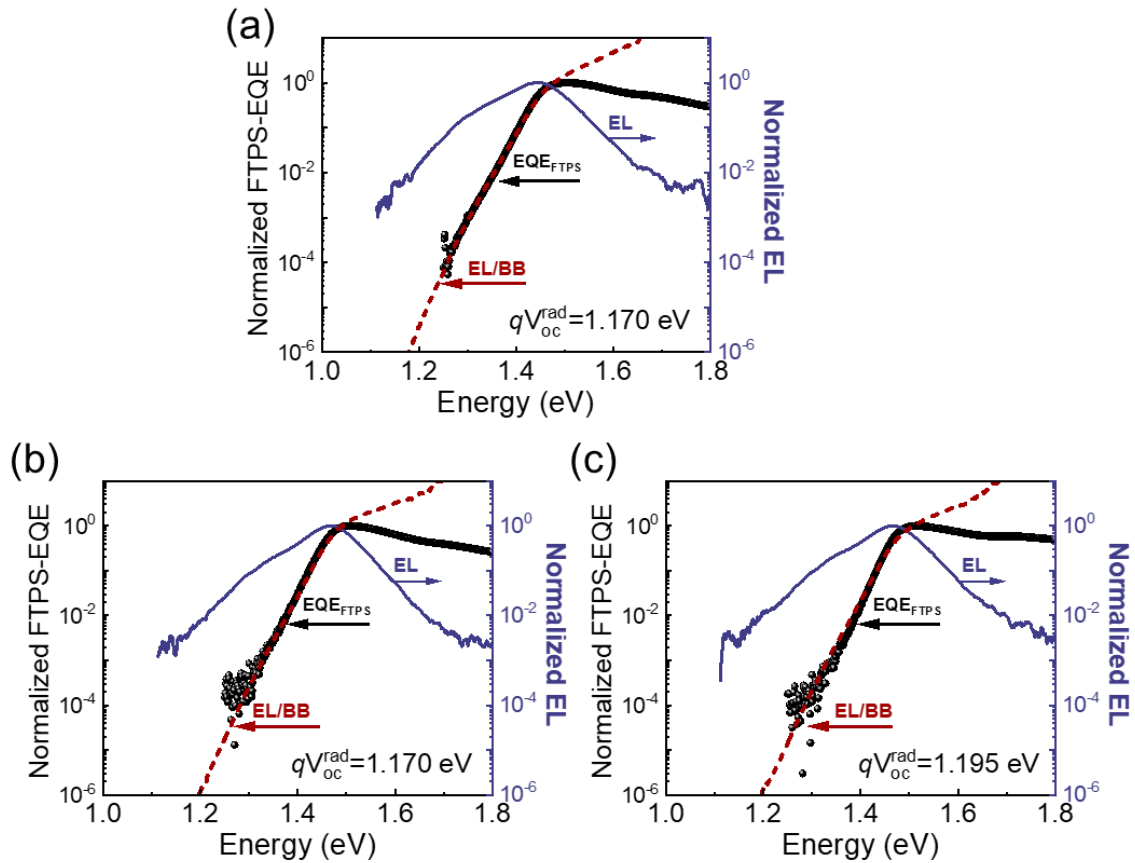


Fig. S14. FTPS-EQE curves of the (a) PM6:MYT, (b) PM6:DYT, and (C) PM6:TYT OSCs.

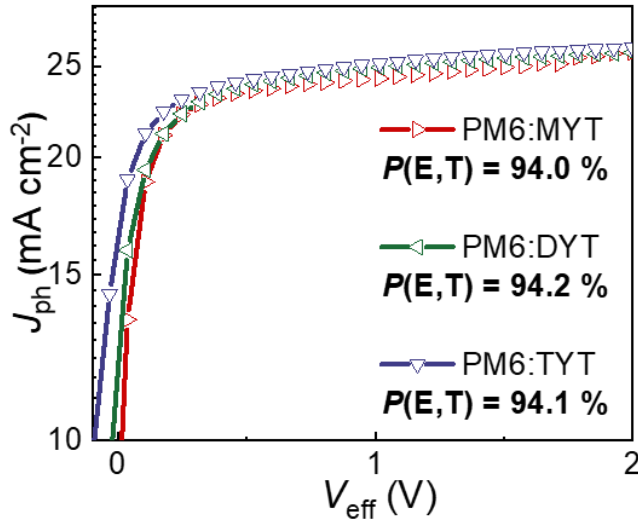


Fig. S15. J_{ph} vs. V_{eff} curves of the PM6:acceptor-based OSCs.

Table S5. SCLC mobilities for the PM6:DSMA blend films.

| Material | μ_h ($\text{cm}^2 \text{V}^{-1} \text{s}^{-1}$) ^a | μ_e ($\text{cm}^2 \text{V}^{-1} \text{s}^{-1}$) ^a | μ_h/μ_e |
|----------|--|--|---------------|
| PM6:MYT | 4.0×10^{-4} | 5.8×10^{-5} | 6.9 |
| PM6:DYT | 4.7×10^{-4} | 3.8×10^{-4} | 1.2 |
| PM6:TYT | 4.5×10^{-4} | 4.2×10^{-4} | 1.1 |

^aAveraged values from 3 independent devices.

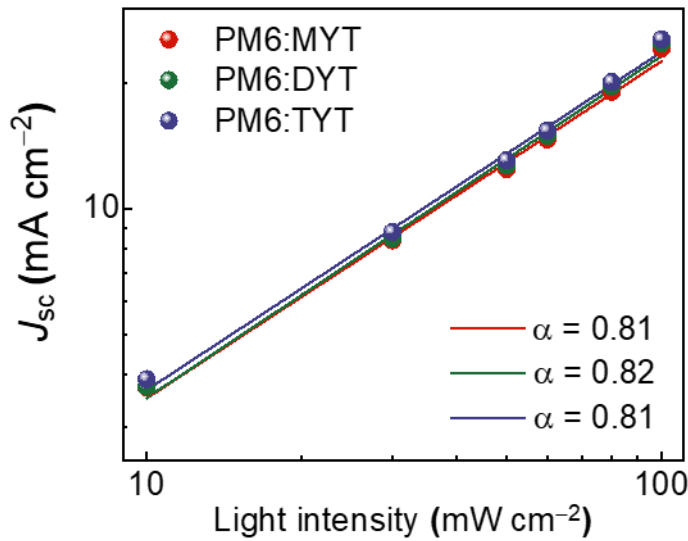


Fig. S16. Light-intensity dependent J_{sc} plots of PM6:acceptor-based OSCs.

Table S6. PCEs at $t_{80\%}$ and $t_{80\%}$ lifetime from photo-stability test of previous works and this work.

| System | Initial PCE (%) | PCE at $t_{80\%}$ (%) | $t_{80\%}$ lifetime (h) | Reference |
|---|-----------------|-----------------------|-------------------------|------------------|
| PTB7-Th:ITIC | 7.28 | 5.82 | 221 | ⁵⁶ |
| PTB7-Th:IDIC | 6.12 | 4.9 | 558 | ⁵⁶ |
| PTB7-Th:EH-IDT | 9.17 | 7.34 | 2132 | ⁵⁶ |
| P3HT:IDTBr | 3.03 | 2.42 | 230 | ⁵⁷ |
| P3HT:IDTBr | 6.05 | 4.84 | 9.2 | ⁵⁷ |
| PM7:IT-4F (ZnO/PET) | 13.19 | 10.55 | 2700 | ⁵⁸ |
| PM6:Y6 (ZnO/PET) | 16.46 | 13.17 | 4410 | ⁵⁸ |
| PBDB-T:PCBM | 5.88 | 4.7 | 7400 | ⁷ |
| PBDB-T:ITIC-2F | 7.78 | 6.22 | 11000 | ⁷ |
| PBDB-T:ITIC-Th | 8.03 | 6.42 | 9500 | ⁷ |
| PM6:Y6 (<i>n</i>-SnO₂) | 13.80 | 11.04 | 100 | ⁵⁹ |
| PM6:Y6 (<i>n</i>-SnO₂/InP/ZnS QDs) | 15.12 | 12.1 | 500 | ⁵⁹ |
| PTB7-Th:IEICO-4F (ZnO) | 9.46 | 7.57 | 2500 | ⁸ |
| PTB7-Th:IEICO-4F (ZnO/C₆₀-SAM) | 10.00 | 8 | 34000 | ⁸ |
| P3HT:PC₆₁BM | 2.89 | 2.31 | 807 | ⁶⁰ |
| PM6:Y6-BO (w/o additives) | 15.1 | 12.08 | 66.2 | ⁶¹ |
| PM6:Y6-BO (w/ DIO) | 16.3 | 13.04 | 6.6 | ⁶¹ |
| PM6:Y6-BO (w/o INB-F) | 16.7 | 13.36 | 523 | ⁶¹ |
| PM6:Y6-BO (w/o INB-Cl) | 16.3 | 13.04 | 120 | ⁶¹ |
| P3HT:IC₆₀BA (ZnO) | 9.95 | 7.96 | 250 | ⁶² |
| P3HT:IC₆₀BA (ZnO/ALD HfO₂) | 10.80 | 8.64 | 750 | ⁶² |
| P3HT:PC₆₁BM (ZnO) | 2.74 | 2.19 | 124 | ⁶³ |
| P3HT:PC₆₁BM (ZnO/PDIN-H) | 2.67 | 2.14 | 780 | ⁶³ |
| PBDB-T:OY3 | 14.87 | 11.90 | 25000 | ⁶⁴ |
| PM6:Y6:20% BTO:PC₇₁BM (PX) | 17.41 | 13.93 | 1000 ^a | ⁶⁵ |
| PM6: TYT | 18.15 | 14.52 | 8415 | This work |

^a $t_{75\%}$ lifetime

Table S7. Lifetime of the PM6:TYT-based OSCs considering annual solar radiations of various countries.

| City (Country) | Latitude (° N) | Longitude (° E) | Annual solar radiation (kWh m ⁻² day ⁻¹) | Lifetime (year) |
|--------------------------------|-------------------|--------------------|---|--------------------|
| Seoul (South Korea) | 37.57 | 127.02 | 4.88 | 4.75 |
| Beijing (China) | 39.89 | 116.38 | 5.16 | 4.49 |
| Washington (USA) | 38.89 | 77.02 | 4.87 | 4.76 |
| Paris (France) | 48.73 | 2.40 | 3.22 | 7.19 |
| London (UK) | 51.15 | 0.18 | 3.09 | 7.50 |
| Berlin (Germany) | 52.47 | 13.40 | 3.00 | 7.72 |

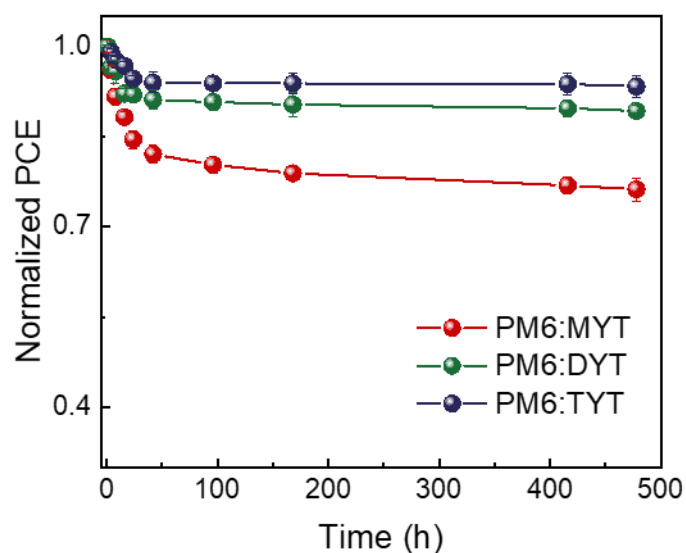


Fig. S17. Thermal stability of PM6:acceptors OSCs under 80 °C.

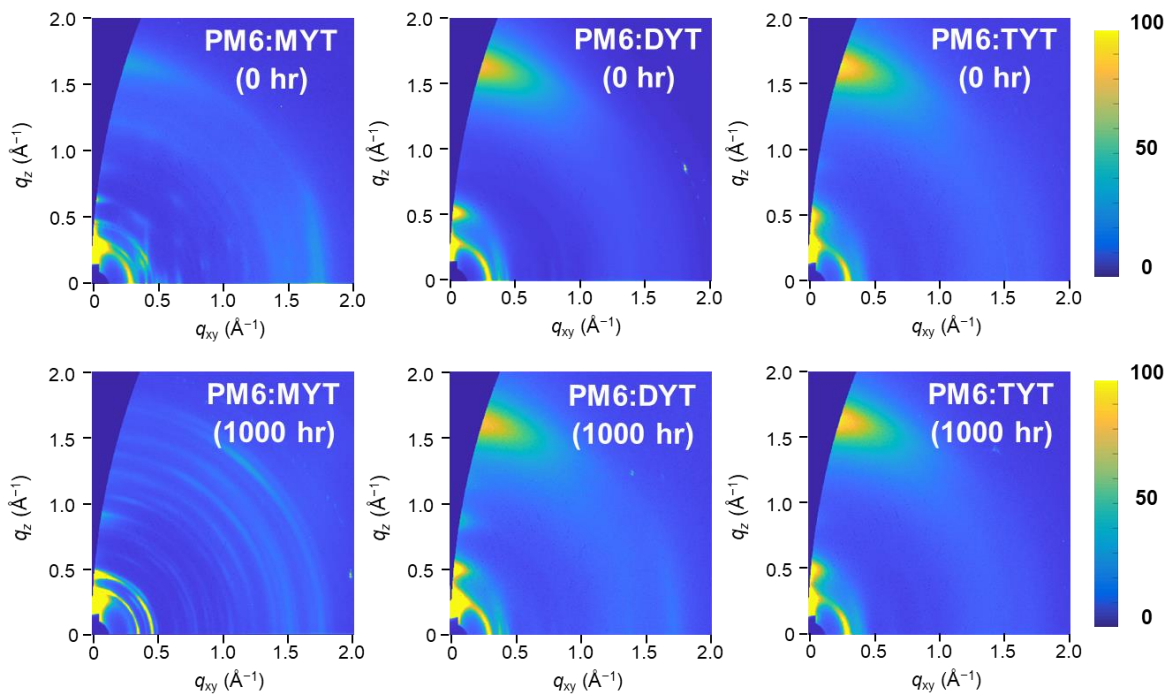


Fig. S18. GIWAXS 2D-images of the PM6:acceptor blend films before and after exposure to light.

Table S8. Domain sizes and relative domain purity of the blend films before and after 1000 hr of illumination.

| System | 0 h | | 1000 h | |
|---------|---------------------|------|---------------------|------|
| | Domain size (nm) | r-DP | Domain size (nm) | r-DP |
| PM6:MYT | 29 | 0.59 | 46 | 1.00 |
| PM6:DYT | 30 | 0.47 | 31 | 0.52 |
| PM6:TYT | 25 | 0.45 | 25 | 0.46 |

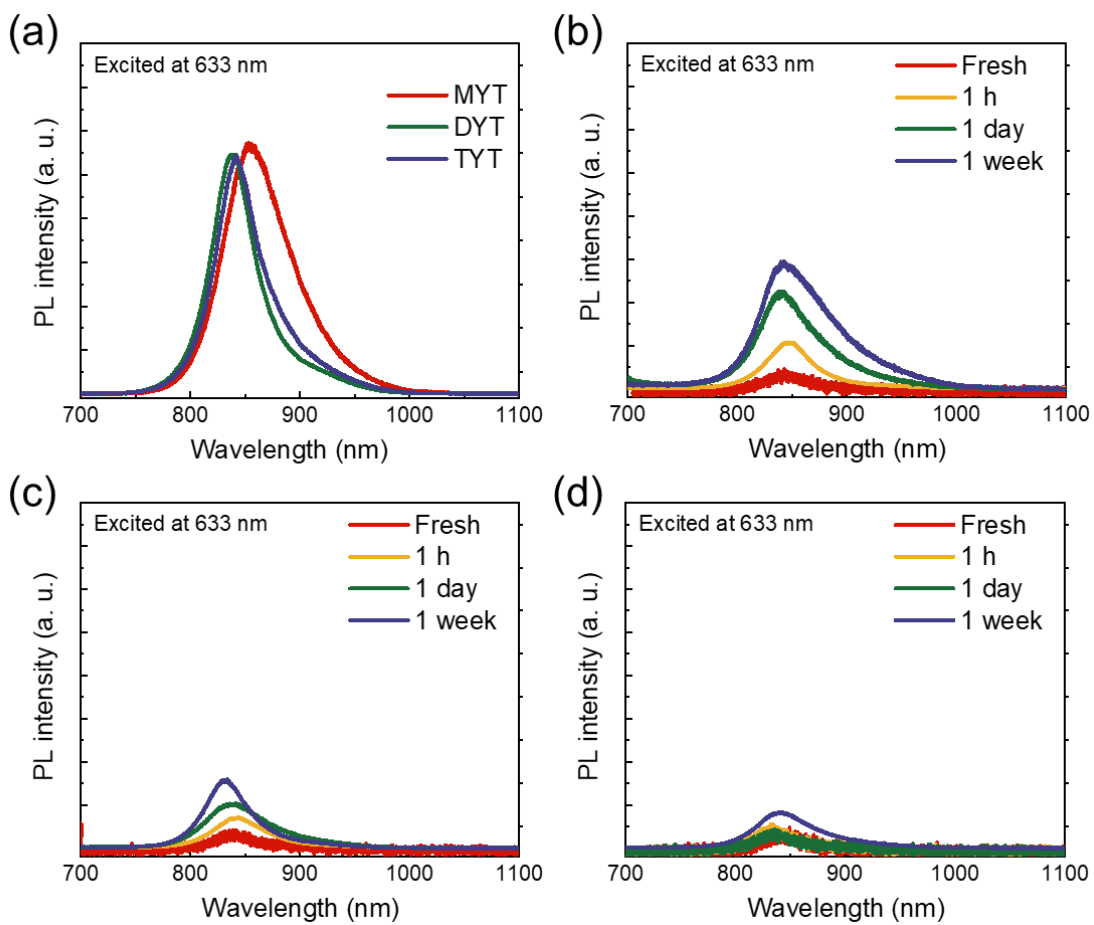


Fig. S19. PL emission spectra of (a) pristine acceptors and (b-d) PM6:acceptor blend films before and after illumination; (b, c, d for PM6:MYT, PM6:DYT, and PM6:TYT, respectively).

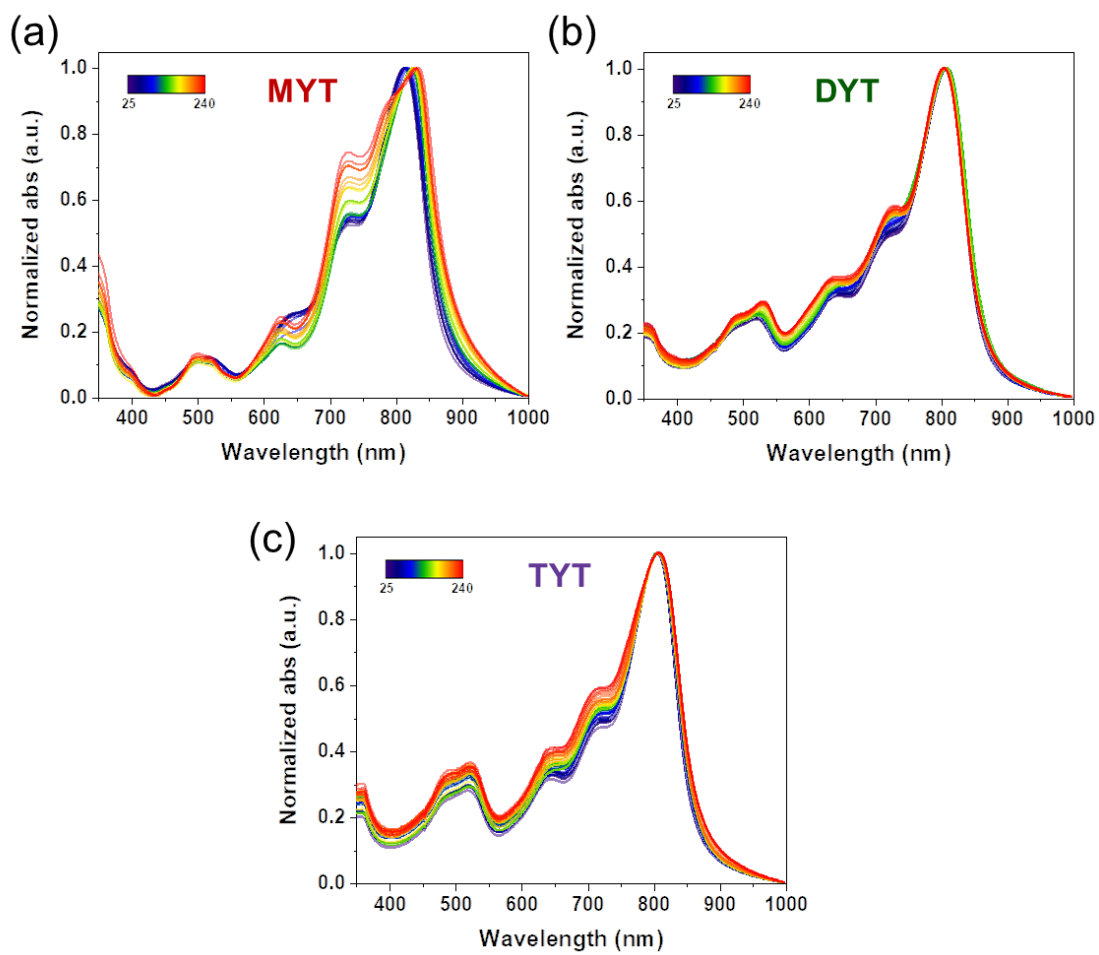


Fig. S20. Film UV-Vis absorption spectra of (a) MYT, (b) DYT, and (c) TYT depending on annealing temperatures (20 – 240 °C).

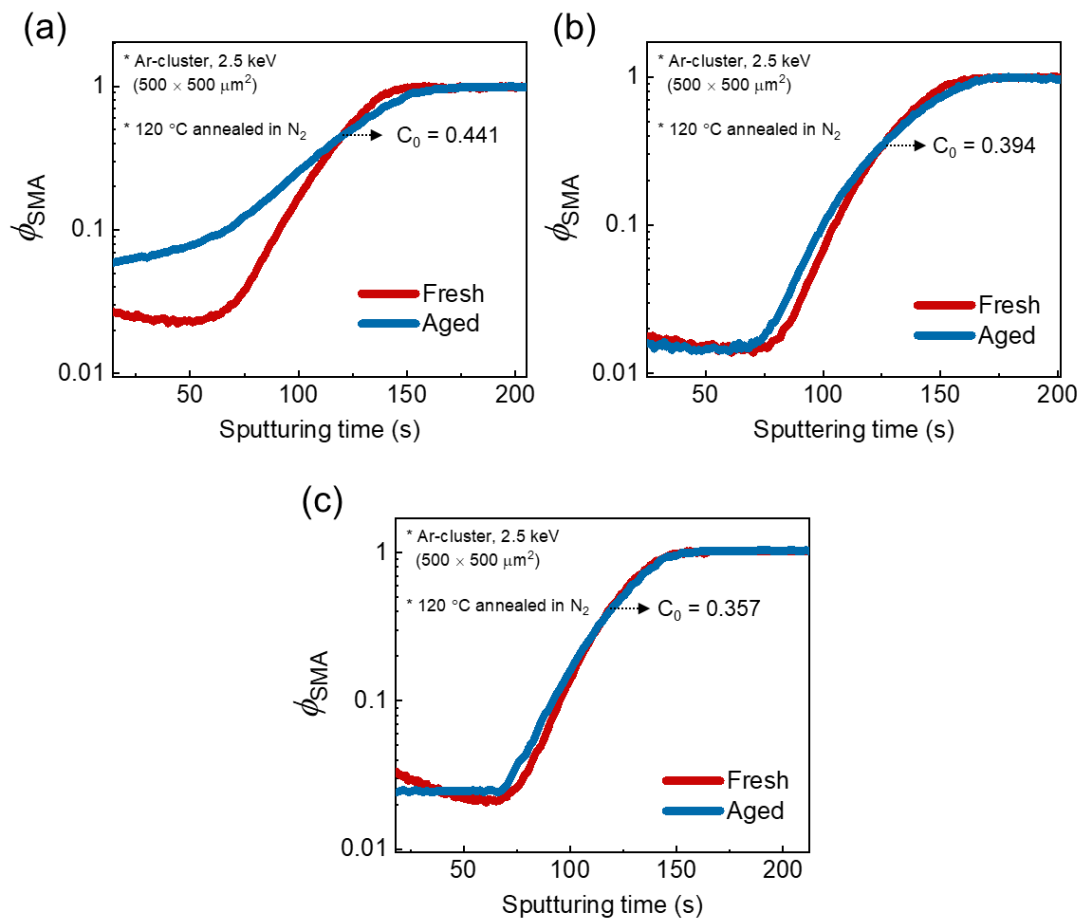


Fig. S21. ToF-SIMS profiles of the (a) PM6:MYT, (b) PM6:DYT, and (c) PM6:TYT blend films, both for fresh films and those thermally treated for one day at 120 °C.

Table S9. D_{120} values for acceptor molecules in blend films with PM6 estimated from the ToF-SIMS profiles.

| Material | $D_{120} (\text{cm}^2 \text{ s}^{-1})$ |
|----------|--|
| MYT | 3.3×10^{-15} |
| DYT | 2.8×10^{-18} |
| TYT | 4.1×10^{-24} |

References

1. J. Yuan, Y. Zhang, L. Zhou, G. Zhang, H.-L. Yip, T.-K. Lau, X. Lu, C. Zhu, H. Peng, P. A. Johnson, M. Leclerc, Y. Cao, J. Ulanski, Y. Li and Y. Zou, *Joule*, 2019, **3**, 1140-1151.
2. S. R. Adusumalli, D. G. Rawale, U. Singh, P. Tripathi, R. Paul, N. Kalra, R. K. Mishra, S. Shukla and V. Rai, *J. Am. Chem. Soc.*, 2018, **140**, 15114-15123.
3. G.-U. Kim, C. Sun, J. S. Park, H. G. Lee, D. Lee, J.-W. Lee, H. J. Kim, S. Cho, Y.-H. Kim, S.-K. Kwon and B. J. Kim, *Adv. Funct. Mater.*, 2021, **31**, 2100870.
4. Y. Li, J. L. Song, Y. C. Dong, H. Jin, J. M. Xin, S. J. Wang, Y. H. Ca, L. Jiang, W. Ma, Z. Tang and Y. M. Sun, *Adv. Mater.*, 2022, **34**, 2110155.
5. Y. Li, J. Song, Y. Dong, H. Jin, J. Xin, S. Wang, Y. Cai, L. Jiang, W. Ma, Z. Tang and Y. Sun, *Advanced Materials*, 2022, **34**, 2110155.
6. J. Yao, B. B. Qiu, Z. G. Zhang, L. W. Xue, R. Wang, C. F. Zhang, S. S. Chen, Q. J. Zhou, C. K. Sun, C. Yang, M. Xiao, L. Meng and Y. F. Li, *Nat. Commun.*, 2020, **11**, 2726.
7. X. Y. Du, T. Heumueller, W. Gruber, A. Classen, T. Unruh, N. Li and C. J. Brabec, *Joule*, 2019, **3**, 215-226.
8. X. Xu, J. Y. Xiao, G. C. Zhang, L. Wei, X. C. Jiao, H. L. Yip and Y. Cao, *Sci. Bull.*, 2020, **65**, 208-216.
9. U. Rau, B. Blank, T. C. M. Muller and T. Kirchartz, *Phys. Rev. Appl.*, 2017, **7**, 044016.
10. W. Shockley and H. J. Queisser, *J. Appl. Phys.*, 1961, **32**, 510-519.
11. T. Kirchartz and U. Rau, *Phys. Stat. Sol.*, 2008, **205**, 2737-2751.
12. S. E. Root, M. A. Alkhadra, D. Rodriguez, A. D. Printz and D. J. Lipomi, *Chem. Mater.*, 2017, **29**, 2646-2654.
13. M. Ghasemi, N. Balar, Z. X. Peng, H. W. Hu, Y. P. Qin, T. Kim, J. J. Rech, M. Bidwell, W. Mask, I. McCulloch, W. You, A. Amassian, C. Risko, B. T. O'Connor and H. Ade, *Nat. Mater.*, 2021, **20**, 525-532.
14. M. Ghasemi, H. W. Hu, Z. X. Peng, J. J. Rech, I. Angunawela, J. H. Carpenter, S. J. Stuard, A. Wadsworth, I. McCulloch, W. You and H. Ade, *Joule*, 2019, **3**, 1328-1348.
15. J. Yuan, Y. Q. Zhang, L. Y. Zhou, G. C. Zhang, H. L. Yip, T. K. Lau, X. H. Lu, C. Zhu, H. J. Peng, P. A. Johnson, M. Leclerc, Y. Cao, J. Ulanski, Y. F. Li and Y. P. Zou, *Joule*, 2019, **3**, 1140-1151.
16. Y. Cui, H. F. Yao, J. Q. Zhang, T. Zhang, Y. M. Wang, L. Hong, K. H. Xian, B. W. Xu, S. Q. Zhang, J. Peng, Z. X. Wei, F. Gao and J. H. Hou, *Nat. Commun.*, 2019, **10**, 2515.
17. K. Jiang, Q. Y. Wei, J. Y. L. Lai, Z. X. Peng, H. Kim, J. Yuan, L. Ye, H. Ade, Y. P. Zou and H. Yan, *Joule*, 2019, **3**, 3020-3033.
18. Y. Cui, H. F. Yao, J. Q. Zhang, K. H. Xian, T. Zhang, L. Hong, Y. M. Wang, Y. Xu, K. Q. Ma, C. B. An, C. He, Z. X. Wei, F. Gao and J. H. Hou, *Adv. Mater.*, 2020, **32**, 1908205.
19. Z. C. Zhou, W. R. Liu, G. Q. Zhou, M. Zhang, D. P. Qian, J. Y. Zhang, S. S. Chen, S. J. Xu, C. D. Yang, F. Gao, H. M. Zhu, F. Liu and X. Z. Zhu, *Adv. Mater.*, 2020, **32**, 1906324.
20. Z. H. Luo, R. J. Ma, Z. X. Chen, Y. Q. Xiao, G. Y. Zhang, T. Liu, R. Sun, Q. Zhan, Y. Zou, C. Zhong, Y. Z. Chen, H. L. Sun, G. D. Chai, K. Chen, X. G. Guo, J. Min, X. H. Lu, C. L. Yang and H. Yan, *Adv. Energy Mater.*, 2020, **10**, 2002649.
21. F. Lin, K. Jiang, W. Kaminsky, Z. L. Zhu and A. K. Y. Jen, *J. Am. Chem. Soc.*, 2020, **142**, 15246-15251.
22. S. Liu, J. Yuan, W. Y. Deng, M. Luo, Y. Xie, Q. B. Liang, Y. P. Zou, Z. C. He, H. B. Wu and Y. Cao, *Nat. Photon.*, 2020, **14**, 300.
23. C. Li, J. D. Zhou, J. L. Song, J. Q. Xu, H. T. Zhang, X. N. Zhang, J. Guo, L. Zhu, D. H. Wei, G. C. Han, J. Min, Y. Zhang, Z. Q. Xie, Y. P. Yi, H. Yan, F. Gao, F. Liu and Y. M. Sun, *Nat. Energy*, 2021, **6**, 605-613.

24. Y. H. Cai, Y. Li, R. Wang, H. B. Wu, Z. H. Chen, J. Zhang, Z. F. Ma, X. T. Hao, Y. Zhao, C. F. Zhang, F. Huang and Y. M. Sun, *Adv. Mater.*, 2021, **33**, 2101733.
25. Y. Z. Chen, F. J. Bai, Z. X. Peng, L. Zhu, J. Q. Zhang, X. H. Zou, Y. P. Qin, H. Kim, J. Yuan, L. K. Ma, J. Zhang, H. Yu, P. C. Y. Chow, F. Huang, Y. P. Zou, H. Ade, F. Liu and H. Yan, *Adv. Energy Mater.*, 2021, **11**, 2003141.
26. F. Qi, K. Jiang, F. Lin, Z. Wu, H. N. Zhang, W. Gao, Y. X. Li, Z. W. Cai, H. Y. Woo, Z. L. Zhu and A. K. Y. Jen, *ACS Energy Lett.*, 2021, **6**, 9-15.
27. B. B. Fan, M. J. Li, D. F. Zhang, W. K. Zhong, L. Ying, Z. M. Y. Zeng, K. An, Z. Q. Huang, L. R. Shi, G. C. Bazan, F. Huang and Y. Cao, *ACS Energy Lett.*, 2020, **5**, 2087-2094.
28. G. D. Chai, J. Q. Zhang, M. G. Pan, Z. Wang, J. W. Yu, J. E. Liang, H. Yu, Y. Z. Chen, A. Shang, X. Y. Liu, F. J. Bai, R. J. Ma, Y. Chang, S. W. Luo, A. P. Zeng, H. Zhou, K. Chen, F. Gao, H. Ade and H. Yan, *ACS Energy Lett.*, 2020, **5**, 3415-3425.
29. C. K. Sun, F. Pan, B. Qiu, S. C. Qin, S. S. Chen, Z. Y. Shang, L. Meng, C. Yang and Y. F. Li, *Chem. Mater.*, 2020, **32**, 3254-3261.
30. Z. Z. Zhang, Y. W. Li, G. L. Cai, Y. H. Zhang, X. H. Lu and Y. Z. Lin, *J. Am. Chem. Soc.*, 2020, **142**, 18741-18745.
31. K. K. Weng, L. L. Ye, L. Zhu, J. Q. Xu, J. J. Zhou, X. Feng, G. H. Lu, S. T. Tan, F. Liu and Y. M. Sun, *Nat. Commun.*, 2020, **11**, 2855.
32. J. E. Liang, M. G. Pan, G. D. Chai, Z. X. Peng, J. Q. Zhang, S. W. Luo, Q. Han, Y. Z. Chen, A. Shang, F. J. Bai, Y. Xu, H. Yu, J. Y. L. Lai, Q. Chen, M. J. Zhang, H. Ade and H. Yan, *Adv. Mater.*, 2020, **32**, 2003500.
33. P. J. Chao, H. Chen, Y. L. Zhu, H. J. Lai, D. Z. Mo, N. Zheng, X. Y. Chang, H. Meng and F. He, *Adv. Mater.*, 2020, **32**, 1907059.
34. X. P. Xu, K. Feng, Z. Z. Bi, W. Ma, G. J. Zhang and Q. Peng, *Adv. Mater.*, 2019, **31**, 1901872.
35. C. K. Sun, F. Pan, S. S. Chen, R. Wang, R. Sun, Z. Y. Shang, B. B. Qiu, J. Min, M. L. Lv, L. Meng, C. F. Zhang, M. Xiao, C. D. Yang and Y. F. Li, *Adv. Mater.*, 2019, **31**, 1905480.
36. S. T. Pang, Z. Q. Wang, X. Y. Yuan, L. H. Pan, W. Y. Deng, H. R. Tang, H. B. Wu, S. S. Chen, C. H. Duan, F. Huang and Y. Cao, *Angew. Chem. Int. Ed.*, 2021, **60**, 8813-8817.
37. G. D. Chai, Y. Chang, J. Q. Zhang, X. P. Xu, L. Y. Yu, X. H. Zou, X. J. Li, Y. Z. Chen, S. W. Luo, B. B. Liu, F. J. Bai, Z. H. Luo, H. Yu, J. E. Liang, T. Liu, K. S. Wong, H. Zhou, Q. Peng and H. Yan, *Energy Environ. Sci.*, 2021, **14**, 3469-3479.
38. Y. L. Ma, M. Zhang, S. Wan, P. Yin, P. S. Wang, D. D. Cai, F. Liu and Q. D. Zheng, *Joule*, 2021, **5**, 197-209.
39. Z. H. Luo, R. J. Ma, T. Liu, J. W. Yu, Y. Q. Xiao, R. Sun, G. S. Xie, J. Yuan, Y. Z. Chen, K. Chen, G. D. Chai, H. L. Sun, J. Min, J. Zhang, Y. P. Zou, C. L. Yang, X. H. Lu, F. Gao and H. Yan, *Joule*, 2020, **4**, 1236-1247.
40. S. X. Li, L. L. Zhan, Y. Z. Jin, G. Q. Zhou, T. K. Lau, R. Qin, M. M. Shi, C. Z. Li, H. M. Zhu, X. H. Lu, F. L. Zhang and H. Z. Chen, *Adv. Mater.*, 2020, **32**, 2001160.
41. W. Gao, H. T. Fu, Y. X. Li, F. Lin, R. Sun, Z. Wu, X. Wu, C. Zhong, J. Min, J. D. Luo, H. Y. Woo, Z. L. Zhu and A. K. Y. Jen, *Adv. Energy Mater.*, 2021, **11**, 2003177.
42. C. Zhu, J. Yuan, F. F. Cai, L. Meng, H. T. Zhang, H. G. Chen, J. Li, B. B. Qiu, H. J. Peng, S. S. Chen, Y. B. Hu, C. Yang, F. Gao, Y. P. Zou and Y. F. Li, *Energy Environ. Sci.*, 2020, **13**, 2459-2466.
43. S. X. Li, L. L. Zhan, N. N. Yao, X. X. Xia, Z. Chen, W. T. Yang, C. L. He, L. J. Zuo, M. M. Shi, H. M. Zhu, X. H. Lu, F. L. Zhang and H. Z. Chen, *Nat. Commun.*, 2021, **12**, 4627.
44. C. Y. Xu, K. Jin, Z. Xiao, Z. J. Zhao, X. L. Ma, X. L. Wang, J. M. Li, W. J. Xu, S. P. Zhang, L. M. Ding and F. J. Zhang, *Adv. Funct. Mater.*, 2021, **31**, 2107934.

45. H. Lu, H. Jin, H. Huang, W. X. Liu, Z. Tang, J. Q. Zhang and Z. S. Bo, *Adv. Funct. Mater.*, 2021, **31**, 2103445.
46. H. Chen, T. X. Zhao, L. Li, P. Tan, H. J. Lai, Y. L. Zhu, X. Lai, L. Han, N. Zheng, L. Guo and F. He, *Adv. Mater.*, 2021, **33**, 2102778.
47. C. Yang, Q. S. An, H. R. Bai, H. F. Zhi, H. S. Ryu, A. Mahmood, X. Zhao, S. W. Zhang, H. Y. Woo and J. L. Wang, *Angew. Chem. Int. Ed.*, 2021, **60**, 19241-19252.
48. C. Q. Tang, X. L. Ma, J. Y. Wang, X. Zhang, R. C. Liao, Y. L. Ma, P. Wang, P. S. Wang, T. Wang, F. J. Zhang and Q. D. Zheng, *Angew. Chem. Int. Ed.*, 2021, **60**, 19314-19323.
49. X. Y. Yuan, Y. L. Zhao, T. Zhan, J. Oh, J. D. Zhou, J. Y. Li, X. J. Wang, Z. Q. Wang, S. T. Pang, P. Cai, C. D. Yang, Z. C. He, Z. Q. Xie, C. H. Duan, F. Huang and Y. Cao, *Energy Environ. Sci.*, 2021, **14**, 5530-5540.
50. H. J. Ning, Q. J. Jiang, P. W. Han, M. Lin, G. Y. Zhang, J. M. Chen, H. Chen, S. Y. Zeng, J. P. Gao, J. G. Liu, F. He and Q. H. Wu, *Energy Environ. Sci.*, 2021, **14**, 5919-5928.
51. Y. Z. Chen, R. J. Ma, T. Liu, Y. Q. Xiao, H. Kim, J. Q. Zhang, C. Ma, H. L. Sun, F. J. Bai, X. G. Guo, K. S. Wong, X. H. Lu and H. Yan, *Adv. Energy Mater.*, 2021, **11**, 2003777.
52. P. Q. Bi, S. Q. Zhang, Z. H. Chen, Y. Xu, Y. Cui, T. Zhang, J. Z. Ren, J. Z. Qin, L. Hong, X. T. Hao and J. H. Hou, *Joule*, 2021, **5**, 2408-2419.
53. Y. Cui, Y. Xu, H. F. Yao, P. Q. Bi, L. Hong, J. Q. Zhang, Y. F. Zu, T. Zhang, J. Z. Qin, J. Z. Ren, Z. H. Chen, C. He, X. T. Hao, Z. X. Wei and J. H. Hou, *Advanced Materials*, 2021, **33**.
54. Y. A. Wei, Z. H. Chen, G. Y. Lu, N. Yu, C. Q. Li, J. H. Gao, X. B. Gu, X. T. Hao, G. H. Lu, Z. Tang, J. Q. Zhang, Z. X. Wei, X. Zhang and H. Huang, *Advanced Materials*, 2022, DOI: ARTN 2204718
10.1002/adma.202204718.
55. W. Gao, F. Qi, Z. X. Peng, F. R. Lin, K. Jiang, C. Zhong, W. Kaminsky, Z. Q. Guan, C. S. Lee, T. J. Marks, H. Ade and A. K. Y. Jen, *Advanced Materials*, 2022, **34**.
56. J. Y. Xiao, M. R. Ren, G. C. Zhang, J. B. Wang, D. L. Zhang, L. L. Liu, N. Li, C. J. Brabec, H. L. Yip and Y. Cao, *Sol. Rrl*, 2019, **3**, 1900077.
57. N. Gasparini, M. Salvador, S. Strohm, T. Heumueller, I. Levchuk, A. Wadsworth, J. H. Bannock, J. C. de Mello, H. J. Egelhaaf, D. Baran, I. McCulloch and C. J. Brabec, *Adv. Energy Mater.*, 2017, **7**, 1700770.
58. Y. F. Han, H. L. Dong, W. Pan, B. W. Liu, X. Z. Chen, R. Huang, Z. Y. Li, F. S. Li, Q. Luo, J. Q. Zhang, Z. X. Wei and C. Q. Ma, *ACS Appl. Mater. Interfaces*, 2021, **13**, 17869-17881.
59. R. X. Peng, T. T. Yan, J. W. Chen, S. F. Yang, Z. Y. Ge and M. T. Wang, *Adv. Electron. Mater.*, 2020, **6**, 1901245.
60. N. Chander, S. Singh and S. S. K. Iyer, *Sol. Energy Mat. Sol. Cells*, 2017, **161**, 407-415.
61. X. Zhang, J. L. Cai, C. H. Guo, D. H. Li, B. C. Du, Y. Zhuang, S. L. Cheng, L. Wang, D. Liu and T. Wang, *Small*, 2021, **17**, 2102558.
62. E. Polydorou, M. Botzakaki, C. Drivas, K. Seintis, I. Sakellis, A. Soultati, A. Kaltzoglou, T. Speliotis, M. Fakis, L. C. Palilis, S. Kennou, A. Fakharuddin, L. Schmidt-Mende, D. Davazoglou, P. Falaras, P. Argitis, C. A. Krontiras, S. N. Georgia and M. Vasilopoulou, *J. Mater. Chem. C*, 2018, **6**, 8051-8059.
63. M. Sadeghianlemraski, C. R. Harding, G. C. Welch and H. Aziz, *ACS Appl. Energy Mater.*, 2020, **3**, 11655-11665.
64. Y. C. Liang, D. F. Zhang, Z. R. Wu, T. Jia, L. Luer, H. R. Tang, L. Hong, J. B. Zhang, K. Zhang, C. J. Brabec, N. Li and F. Huang, *Nat. Energy*, 2022, **7**, 1180–1190.

65. H. Y. Chen, R. Zhang, X. B. Chen, G. Zeng, L. Kobera, S. Abbrent, B. Zhang, W. J. Chen, G. Y. Xu, J. Oh, S. H. Kang, S. S. Chen, C. Yang, J. Brus, J. H. Hou, F. Gao, Y. W. Li and Y. F. Li, *Nat. Energy*, 2021, **6**, 1045-1053.